Journal of Energy Storage 175 (2026) 123284

Contents lists available at ScienceDirect

Journal of Energy Storage

journal homepage: www.elsevier.com/locate/est

Review Article

Expanded graphite–epoxy reinforced composite phase change materials for thermal management of electric vehicle batteries: A critical review

R.M. Ghogare, D.D. Deshmukh *

MET's Institute of Engineering, SPPU, Pune, MS, India

ARTICLE INFO

Keywords:
Battery thermal management system
Phase change material
Expanded graphite
Epoxy resin
Composite PCM
Thermal runaway
Electric vehicle
Lithium-ion battery

ABSTRACT

The rapid global proliferation of electric vehicles (EVs) with sales growing 55-fold between 2014 and 2024 and constituting 22% of global passenger car sales in 2024 has intensified demand for reliable, safe, and energy-efficient battery thermal management systems (BTMS). Lithium-ion batteries (LIBs) operate optimally within a narrow temperature window of 15–35 °C; excursions beyond this range accelerate aging, reduce capacity, and in extreme cases trigger catastrophic thermal runaway (TR). Phase change materials (PCMs) offer passive, latent-heat-based buffering that is inherently parasitic-power-free, yet their intrinsically low thermal conductivity (~0.2 W m^{-1} K^{-1}) and leakage susceptibility limit practical deployment. Expanded graphite (EG) provides a three-dimensional porous scaffold that simultaneously enhances thermal conductivity by up to 100-fold and suppresses liquid-phase leakage; epoxy resin (ER) further imparts structural integrity, electrical insulation, and flame retardancy. This review critically synthesises 145+ peer-reviewed publications to (i) establish the thermophysical and safety performance landscape of EG/ER-composite PCMs (CPCMs), (ii) benchmark key formulations against alternative BTMS modalities, and (iii) identify remaining technical barriers and future research pathways.

1. Introduction

1.1. Global EV market trajectory and LIB technology evolution

The escalating demand for safe, energy-efficient, and long-lasting electric vehicle (EV) battery systems has made battery thermal management one of the most active frontiers in materials science and engineering. CPCMs based on EG and ER have emerged as leading compositions for passive BTMS owing to their simultaneous gains in thermal conductivity, mechanical integrity, and flame retardancy. Among recent experimental demonstrations, Reddy et al. [1] reported a thermal conductivity of 27.10 W m^{-1} K^{-1} for an EG-integrated CPCM, accompanied by compressive and tensile strengths of 39.4 MPa and 9.0 MPa, respectively, enabling cell surface temperatures to remain below 42 °C under high-load operation, a substantial improvement over conventional systems where temperatures exceed 52 °C. Complementing this, Zhang et al. [2] demonstrated that a sulfur-free EG/paraffin CPCM achieves a latent heat of 253.08 J g^{-1} with an EG expansion volume of 324 mL/g, delivering high thermal energy storage capacity while eliminating corrosive sulfur residues from the fabrication process.

From a system-level perspective, Luo et al. [3] demonstrated that a novel dual-phase PCM composite coupled with a graphite film (in-plane thermal conductivity of 1400 W m^{-1} K^{-1}) and epoxy resin in a 5:2:3 mass ratio maintained the maximum battery temperature at only 33 °C with a pack temperature non-uniformity ΔT of just 1.4 °C at 4 C discharge, rising to only 44.8 °C after six consecutive extreme fast-charging cycles, satisfying the most demanding thermal design targets. Addressing the equally critical safety dimension, Pea et al. [4] showed that an epoxy resin/aluminium trihydroxide (ATH)/EG ternary composite achieved UL-94 V-0 flame classification, 67.33% reduction in peak heat release rate (PHRR), and 50.38% reduction in total heat release (THR) in cone calorimetry, while simultaneously improving compressive modulus by 400.12% and maintaining thermal stability to 800 °C, making it among the most comprehensively validated flame-retardant CPCMs reported to date. These four landmark results [1–4] collectively define the current state-of-the-art performance envelope for EG/epoxy CPCMs and motivate the systematic critical review presented herein.

At the market level, the global EV sector has undergone unprecedented expansion, with EV sales increasing nearly 55-fold between 2014

* Corresponding author.
E-mail address: dhirgajanan@gmail.com (D.D. Deshmukh).

https://doi.org/10.1016/j.est.2026.123284
Received 9 January 2026; Received in revised form 28 May 2026; Accepted 22 June 2026
Available online 26 June 2026

and 2024 and more than sixfold since 2020 alone, constituting approximately 22% of total global passenger vehicle sales by 2024 [5]. This rapid adoption trajectory has intensified research and development activities across advanced battery materials, thermal management systems, and energy-efficient vehicle architectures. Among various materials used in EV battery systems, epoxy-based composite structures reinforced with hybrid ceramic fillers have demonstrated enhanced thermogravimetric stability and superior thermal resistance, thereby confirming the suitability of epoxy resin as an effective structural matrix for high-temperature battery pack encapsulation and thermal management applications [6]. Simultaneously, the EV industry has emerged as a major catalyst for technological innovation and sustainable advancements across the entire automotive supply chain [7]. However, environmental and climatic factors significantly influence EV adoption rates. Studies indicate that extremely low ambient temperatures adversely affect EV market penetration more severely than high temperatures, following an inverted U-shaped relationship with temperature variation [8].

From a broader systems perspective, policy support mechanisms, consumer acceptance, and the availability of charging infrastructure have been identified as the primary driving forces governing the adoption trajectory of new energy vehicles [9]. Under favourable policy implementation scenarios, EV penetration in China is projected to reach 27.31%, 42.40%, and 52.97% by the years 2025, 2030, and 2035, respectively [10]. Furthermore, spatial econometric analyses of pure EV sales in China reveal significant positive spatial autocorrelation among provinces, indicating that adoption in neighbouring regions positively influences local EV penetration rates through spillover effects [11]. Based on provincial development characteristics, China's EV ecosystem has been categorised into four major clusters, namely producers, retailers, green-transport leaders, and lagging regions [12]. Additionally, network-based investigations of the new energy vehicle sector demonstrate that organisations occupying central positions within collaborative innovation networks exhibit enhanced technological competitiveness and higher innovation output, with collaboration density being positively correlated with technological advancement [13].

At the battery system level, substantial progress has been achieved in LIB technologies through the development of advanced cathode chemistries such as nickel–manganese–cobalt oxide (NMC811), nickel cobalt aluminium oxide (NCA), and lithium iron phosphate (LFP), along with silicon-composite anodes and improved electrolyte systems. Parallel advancements in battery management systems (BMS) have resulted in the integration of sophisticated state estimation algorithms, including robust extended Kalman filters (EKF), iterative particle swarm optimisation-based EKF, and adaptive unscented Kalman filters capable of maintaining state-of-charge estimation errors below 1%. Furthermore, star-structured LC resonant switched-capacitor balancing circuits have demonstrated cell-balancing efficiencies exceeding 98% [14]. Emerging artificial intelligence and machine learning approaches have further accelerated battery diagnostics and prognostics. Transformer-based deep learning frameworks, such as the patch cross-variate Transformer (Patch CVT), trained using real-world EV operational datasets, have achieved state-of-health estimation root-mean-square errors as low as 0.729% following self-supervised pre-training [15]. Despite these advancements, real-time diagnostics and monitoring of battery thermal behaviour remain significant unresolved research challenges [16].

In parallel, the end-of-life management and recycling of LIB materials have become increasingly important due to the growing volume of spent batteries generated from EV applications. Hydrometallurgical, pyrometallurgical, and direct recycling methodologies have emerged as the primary approaches supporting circular economy strategies for sustainable next-generation battery systems [17]. Moreover, data-driven electrothermal modelling techniques have demonstrated prediction accuracies exceeding 90% using only the initial 100 operational cycles of battery data, thereby enabling early-stage performance prediction and health assessment [18]. Comprehensive reviews on BTMS have further highlighted the prospects and limitations associated with air cooling, liquid cooling, phase change materials, and hybrid thermal management approaches. Among these, minimisation of parasitic power consumption and achieving uniform temperature distribution within battery packs remain the most critical unresolved technical barriers for efficient EV battery thermal management [19,20]. Fig. 1 illustrates the correlated growth trajectory of EV market penetration and BTMS research publication volume from 2014 to 2024, confirming that intensifying commercial demand has directly driven proportional escalation of BTMS research activity [5].

1.2. *Thermal management challenges in lithium-ion batteries*

Despite advances in cell chemistry, LIBs face inherent thermal management constraints. Exothermic electrochemical reactions cause temperature increases that accelerate degradation, modify reaction kinetics, and ultimately threaten safety [21]. Comprehensive reviews of PCM-based BTMS affirm that PCM systems offer the most favourable balance of thermal buffering capacity, weight, and simplicity among passive approaches [22,23]. The synergism of PCM and liquid cooling has been shown to enhance heat dissipation characteristics substantially compared to either method alone, with the hybrid strategy enabling more uniform temperature distribution across the battery pack [24]. Canopy-to-canopy constructal liquid cooling demonstrates that tree-shaped channel networks can achieve superior temperature uniformity with lower pumping power compared to conventional parallel-channel designs [25]. Carbon materials in lithium-ion and post-lithium-ion batteries including graphene, carbon nanotubes, and graphite continue to be intensively studied for their dual role as electrochemically active components and thermally conductive additives [26]. Nano-enhanced PCMs incorporating metal-oxide nanoparticles demonstrate significant improvements in thermal conductivity without severely penalising latent heat, establishing a promising direction for BTMS applications [27]. Mathematical modelling and simulation of photovoltaic thermal systems provides methodology transferable to coupled electrochemical-thermal BTMS simulation [28]. BTMS designs integrating PCM with heat pipes demonstrate that PCM effectively reduces temperature differences within the battery pack while heat pipes provide continuous heat dissipation pathways, with temperature uniformity improvements of up to 30% under optimised configurations [29]. Advances in electrospun nanofiber materials for post-lithium-ion batteries contribute to the fundamental understanding of carbon network architectures applicable to EG scaffold design [30]. Thermal design criteria for EV packs mandate cell surface temperatures of 15–35 °C, maximum temperature differences (ΔT) below 5 °C, and TR onset temperatures substantially above normal operating conditions. Meeting these criteria simultaneously under aggressive drive cycles, fast charging, and extreme ambient temperatures demands a multi-layer thermal management strategy. Fig. 2 summarises the principal thermal management challenges in LIB systems, encompassing the competing requirements of heat dissipation, temperature uniformity, TR prevention, and system-level weight and cost constraints.

1.3. *Thermal runaway: mechanisms, propagation, and safety implications*

Thermal runaway constitutes a self-sustaining, self-accelerating exothermic cascade. Oxygen release from delithiated nickel-rich cathodes triggers exothermic electrolyte oxidation above 180 °C, releasing 800–1200 J g^{-1} of cathode material [31]. At the module level, average TR propagation time at a 3 C charging rate equals only 12.1% of that at 0.5 C, with the lowest TR onset temperature reaching 127.4 °C; air-mediated heat conduction accounts for 67% of total inter-cell heat transfer [32]. These metrics underscore the urgency of passive-first thermal barriers capable of delaying onset, suppressing propagation, and self-extinguishing under ignition. Fig. 3 quantifies the TR

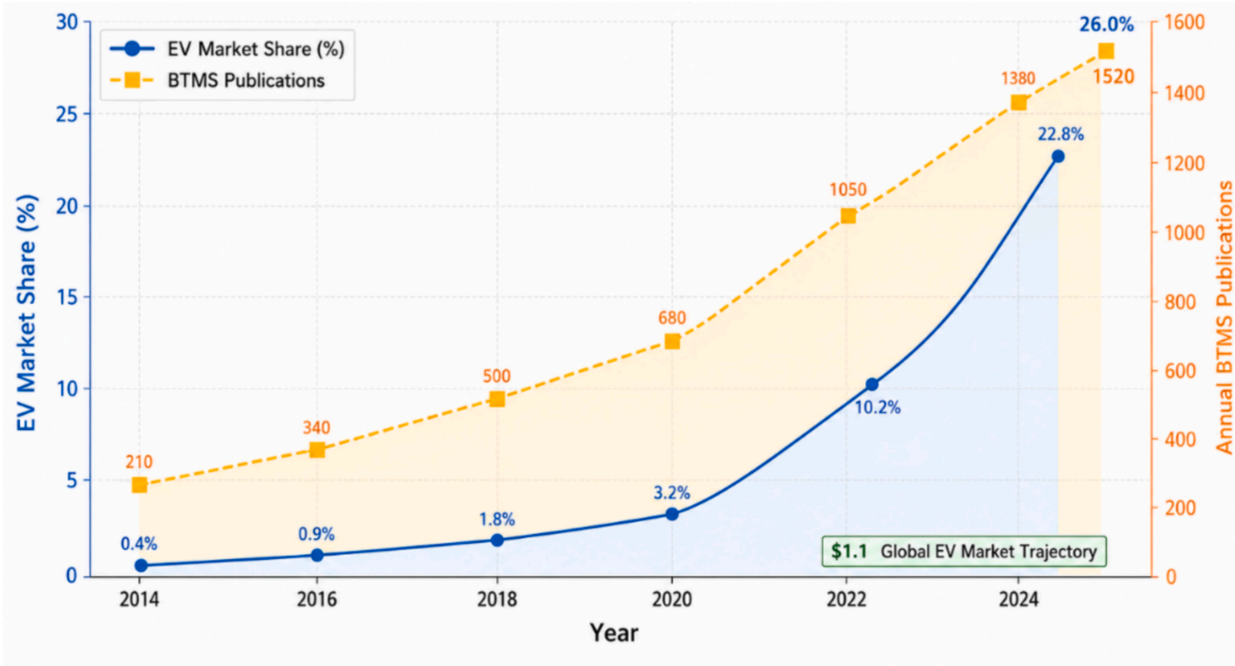

Fig. 1. EV market growth and BTMS research correlation (EV sales increased 55-fold between 2014 and 2024) [5].

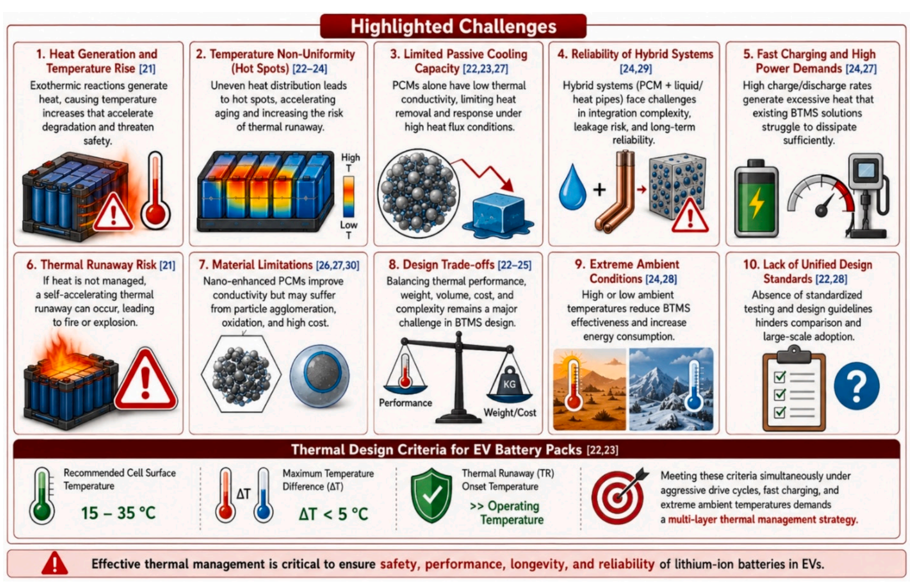

Fig. 2. Thermal management challenges in LIB.

propagation rate as a function of C-rate for a LIB module under overcharge conditions, demonstrating the exponential acceleration of intercell heat transfer at higher charge rates and confirming that passive CPCM barriers must be designed to withstand the most severe fast-charging scenarios [32].

1.4. Phase change materials: classification and current status

PCMs exploit the latent heat of solid-liquid phase transitions to absorb large quantities of thermal energy isothermally, making them inherently suited to passive BTMS. A bibliometric analysis of 583 PCM publications from 2006 to 2022 reveals a progressive shift toward inorganic materials, although organic paraffins and polyethylene glycols remain dominant due to facile production, tunable melting points, and chemical stability [33,34]. PCM-based BTMS for electric and hybrid vehicles demonstrates lightweight, high thermal homogeneity, and compact design advantages over conventional active cooling methods, with multi-layer PCM configurations capable of further reducing system mass and cost [23]. Hybrid BTMS combining PCM with micro heat pipe arrays and intermittent water spraying has demonstrated maximum temperature control to 29.6 °C with non-uniformity below 1.6 °C under dynamic EV drive cycle conditions, with total energy consumption amounting to only 1.8% of battery pack capacity [35]. Composite PCM-based BTMS reviews highlight that combining PCM cooling with air or liquid further improves both cooling efficiency and temperature uniformity, with coupled cooling consistently outperforming single-modality approaches [36]. In-situ polymerisation of solid-state electrolytes represents an emerging cell chemistry trend that will impose new

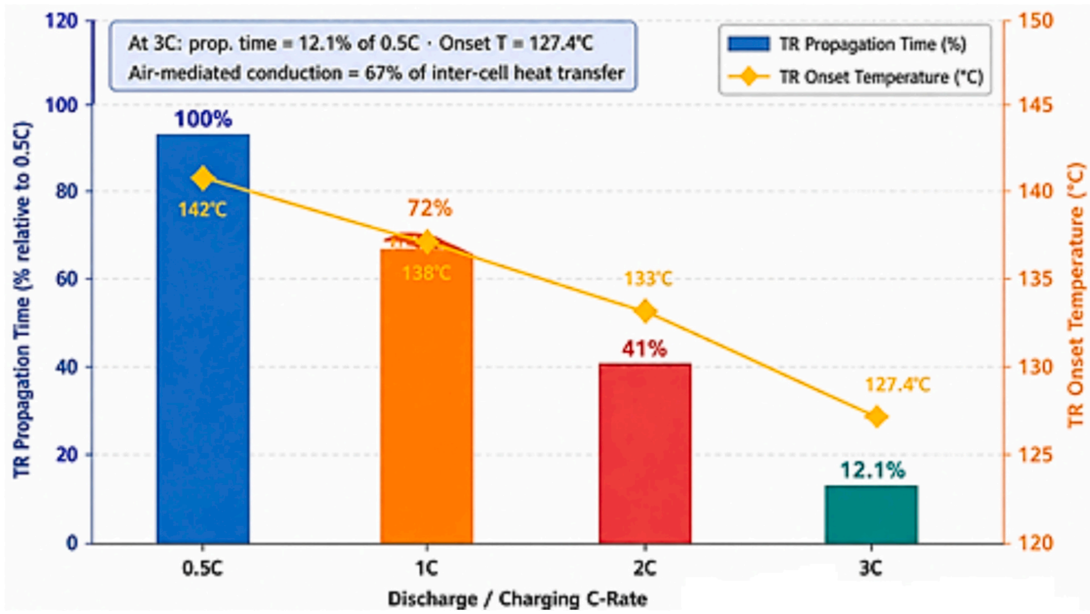

Fig. 3. TR propagation rate vs C rate LIB module overcharge [32].

thermal management requirements on next-generation battery packs [37]. Fin-integrated PCM BTMS studies confirm that optimised fin configurations reduce both maximum temperature and temperature non-uniformity compared to unfinned PCM systems, with design guidelines applicable to composite EG/epoxy CPCM geometries [38]. Recent progress on composite PCM-based BTMS underscores that ultrasonic monitoring, machine learning, and IoT-enabled real-time control represent the most impactful near-term directions for commercial deployment [39]. Key limitations low thermal conductivity (~0.2 W m^{-1} K^{-1}), leakage upon melting, supercooling, and volume expansion have motivated extensive composite engineering [40]. Fig. 4 presents the hierarchical classification of PCMs relevant to EV BTMS, distinguishing organic (paraffins, fatty acids, polyethylene glycols), inorganic (salt hydrates, metallic alloys), and eutectic categories, alongside their respective thermophysical property ranges and principal limitations that drive composite EG/epoxy CPCM development.

This review critically examines the state of the art in EG- and epoxy-reinforced CPCMs for EV BTMS through systematic synthesis of literature published from 2019 to 2025. Complementary reviews of PCM application in EV battery pack thermal management [41], recent BTMS performance enhancement techniques with nano-enhanced PCMs [42], and thermal management of Li-ion batteries using PCMs encompassing future challenges [43] collectively delineate the broader landscape within which the present EG/epoxy-specific analysis is situated. Aerogel fibre technology [44] and graphene-enhanced CPCMs [45] represent adjacent material innovation streams that inform scaffold engineering principles applicable to EG composites. Section 2 establishes the fundamental heat generation and thermal runaway physics. Section 3 classifies BTMS approaches with quantitative benchmarking. Sections 4–7 detail PCM evolution, EG scaffold properties, epoxy matrix functions, and synergistic EG/epoxy formulations. Section 8 surveys experimental and computational characterisation methods. Section 9 addresses system-level integration and TR suppression. Section 10 examines sustainability and scalability. Section 11 identifies remaining

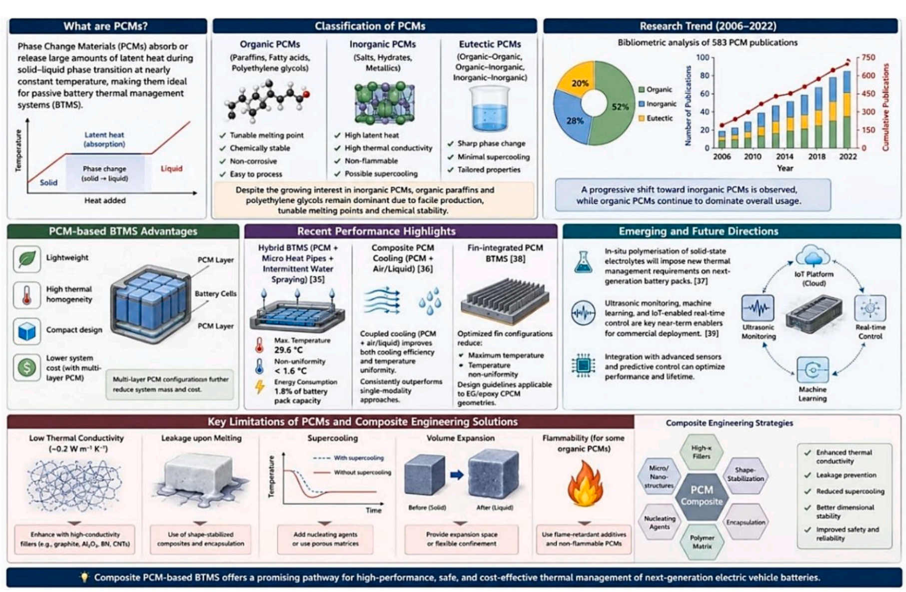

Fig. 4. Phase change materials: classification and current status.

barriers and future directions.

2. Fundamentals of heat generation and thermal issues in EV LIB

2.1. Heat generation mechanisms

LIBs generate heat through an intrinsically coupled electrochemical-thermal process comprising irreversible Joule heating, reversible entropic heat, and contact/solid-electrolyte interphase (SEI) layer resistance. A pseudo-two-dimensional electrochemical-thermal model implemented in COMSOL Multiphysics for NMC811 cells demonstrates that at a 5 C discharge rate, maximum temperature reaches 56.8 °C at the electrode-electrolyte interface with a coefficient of variation of 20.2%, driven by 12% strain-induced heat generation increase and 10% internal resistance increase from hydrofluoric acid (HF) formation [46]. The average volume-weighted temperature escalates from 33.5 °C at 1 C to 53.6 °C at 5 C discharge, with minimum surface temperatures ranging from 32.5 °C at 1 C to 50.5 °C at 5 C, reflecting limited heat dissipation due to low electrolyte thermal conductivity [46]. Sensitivity analyses reveal that ±20% variations in electrolyte decomposition rate alter thermal gradients by 0.9–1.3 °C. Mitigation strategies validated in the same study include cobalt-rich surface coatings that reduce heat generation by 8–12% at 5 C, and vinylene carbonate (VC) additives that suppress HF formation by 15–20% and lower capacity fade by 10% after 200 cycles [46]. In-situ microcalorimetry of LFP cells demonstrates that heat flow after 100, 200, and 300 aging cycles decreases by 45.13%, 40.84%, and 34.89%, respectively, relative to fresh cells, with a weak exothermic anomaly emerging during discharge after 300 cycles [47]. Under low temperature-rise conditions, cell heat generation follows a 'fast-slow-fast' trend; under high temperature-rise conditions, a U-shaped pattern emerges, with mean heat generation rate increasing with decreasing temperature and increasing discharge rates [48].

2.2. Temperature effects on performance, aging, and safety

Temperature critically influences electrochemical kinetics, ionic transport, and SEI evolution. Lithium plating which drastically reduces battery life and limits fast-charging capability occurs under three primary conditions: low-temperature charging, high C-rate charging, and overcharging, with initiation at discharge rates as low as 0.2 C at −20 °C in commercial cells; in severe cases, lithium dendrites penetrate the separator, inducing internal short circuits [49].

Non-uniform temperature distributions impose additional aging penalties: cycling at 3 C with non-uniform distributions produces aging equivalent to operation at the maximum uniform temperature, with cells maintained at 40 °C exhibiting 30% greater capacity loss than those cycled individually [50]. Contrary to intuition, cells subjected to maintained temperature gradients exhibit lower impedance than cells held at the theoretical average temperature, attributable to the non-linear temperature dependence of charge transfer resistance [51].

2.3. Thermal runaway mechanisms and propagation

TR constitutes a self-sustaining process wherein internal heat generation exceeds heat dissipation, triggering sequential exothermic reactions. Transition metal dissolution from cathode films driven by delithiation-induced structural instability is a primary initiating mechanism that degrades electronic conductivity prior to thermal runaway onset [52]. In prismatic 156 Ah NMC811 cells, TR generates an energy increase of 2.5–2.9 MJ, with 31–40% retained in the cell and 60–69% discharged via venting components; of the vented energy, 55–63% is associated with ejected particles, of which a minimum of 88% by mass have diameter ≤1 mm [53] (Fig. 5). Comparative studies on TR characteristics of LFP battery modules under different overcharge conditions reveal that higher overcharge multipliers accelerate heat accumulation and reduce onset time, underscoring the importance of protective BTMS barriers [54]. A novel integrated liquid channel/aerogel structure mitigates TR propagation at a mass flow rate of 4×10^{-6} kg/s — 7-fold lower than the 2.8×10^{-5} kg/s required for conventional single liquid cooling plates [55]. Increasing aerogel thickness reduces the battery-surface heat transfer ratio from 66% to 44%; increasing mass flow rate reduces it from 74% to 42% [55].

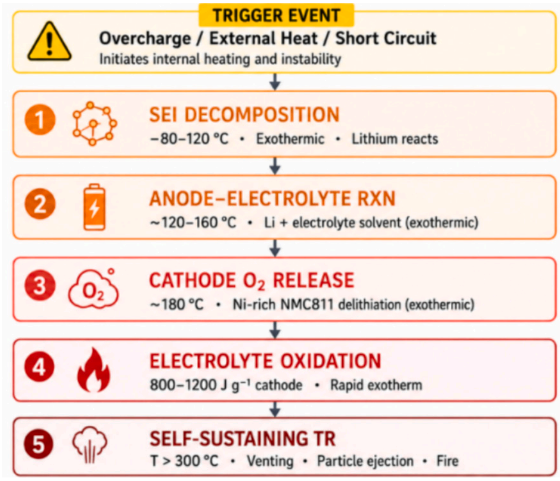

Fig. 5. Thermal runaway cascade mechanism (156 Ah NMC811 cells).

2.4. Quantitative thermal design criteria

Industry-standard thermal design criteria for EV battery packs specify: (i) cell surface temperature maintained at 15–35 °C under normal operation; (ii) $\Delta T \leq 5$ °C across the pack; (iii) TR onset temperature well above 60 °C operational ceiling; and (iv) TR propagation suppression for a minimum delay of 5 min to allow occupant egress. Battery EV thermal management system modelling and validation studies confirm that these criteria can be achieved simultaneously through properly designed multi-layer BTMS architectures combining passive and active elements [56]. System-level thermal management design frameworks for battery EV establish that passive-first architectures with active augmentation represent the optimal trade-off between cost, weight, and thermal performance across a wide range of drive cycles [57]. Three-dimensional COMSOL simulations demonstrate that increasing thermal barrier specific heat capacity by 60% delays TR propagation time by approximately 26%, while anisotropic thermal conductivity increases the critical suppression threshold by approximately 28% compared to isotropic barriers [58].

3. Classification of BTMS

EV battery thermal management systems can be divided into active system, passive system and hybrid system according to energy consumption, complexity, and control considerations. Each category exhibits distinct strengths and weaknesses across the key performance indicators, including temperature uniformity, energy penalty, weight addition, cost (implementation, operational and maintenance), reliability, and compatibility with fast-charging. The initial implementation cost represents the upfront expenditure associated with system design, installation, hardware integration, sensors, pumps, heat exchangers, PCM encapsulation, and control units. The operational energy cost refers to the parasitic power consumed during BTMS operation, such as energy required for pumps, compressors, fans, or thermoelectric modules, which directly affects EV driving range and energy efficiency. The maintenance and complexity cost accounts for long-term servicing, replacement of components, system reliability, and operational complexity associated with cooling circuits and control strategies.

Active BTMS generally exhibit higher operational and maintenance costs, passive BTMS show minimal operational cost due to zero external energy requirement, while hybrid BTMS involve higher implementation complexity but provide superior thermal regulation and fast-charging compatibility. Fig. 6 presents a hierarchical classification of BTMS based on energy consumption, categorising systems into active, passive, and hybrid configurations.

3.1. Active BTMS

Active systems utilise external power sources to circulate cooling or heating media. Indirect liquid cooling represents an efficient technique for maintaining battery temperature at a desired state with minimal energy consumption [59]. Air-cooled staggered configurations produce lower and more uniform temperature distributions than aligned arrangements, but cannot maintain ΔT below 8 °C under 3 C discharge in 60 kWh packs at 40 °C ambient temperature [60]. Two-phase immersion cooling based on pool boiling for 4680 LIB packs maintains cell temperature consistently at 34–35 °C throughout alternating charge/discharge cycles, with enhanced surface roughness improving boiling heat transfer performance [61]. A hybrid thermoelectric-PCM-liquid BTMS achieves dual functionality power generation and cooling with passive cooling maintaining T_max below 323.15 K with ΔT under 5 K for 1 C–4 C discharge; a 340-s delayed activation strategy for active cooling extends thermoelectric generator operation and reduces active cooling duration by 47.2% [62].

3.2. Passive BTMS

Passive systems operate with zero parasitic power consumption. PCM-based temperature regulation is particularly beneficial during fast charging or high-rate discharge [34]. PCM-fin systems exhibit superior temperature management compared to pure PCM alone; optimal configuration comprises one cylindrical ring and eight longitudinal fins with dimensionless spacing of 0.2, with fin structures performing better at higher heat generation rates, though increasing the number of fins beyond eight reduces PCM volume and shortens effective thermal buffering duration [63]. Oscillating heat pipes (OHP) with an optimal Do/Di of 2 mm/1 mm and filling ratio of 9.8% maintain average heater surface temperature at 56.4 °C under 14 W heating power with 25 °C coolant [64]. Heat-pipe-assisted air cooling of lithium-titanate prismatic batteries achieves effective temperature regulation while avoiding the complexity of liquid cooling circuits, confirming heat pipes as a viable passive-first element for BTMS [65]. Shape memory alloy-based passive interfacial thermal regulators offer reversible switching between high and low thermal conductance states in response to temperature, enabling passive self-regulating thermal management without parasitic power consumption [66]. Temperature and aging studies of LIBs confirm that maintaining cells within the optimal temperature window through passive means substantially extends cycle life and reduces capacity fade rates [67]. Heat pipe thermal management for LIBs, when designed with optimal filling ratio and working fluid selection, provides effective isothermalisation of cell surfaces with minimal additional mass [68].

3.3. Hybrid BTMS

Hybrid architectures integrate the high heat absorption capacity of passive elements with the superior temperature uniformity of active cooling. A hybrid TMS combining air cooling, PCM, six flat heat pipes, and a thin aluminium heat sink reduces maximum temperature from 59.8 °C to 36.18 °C a 39.5% improvement with a temperature difference of approximately 0.64 °C across a four-cell module [69]. PCM alone achieves only 40.8 °C and heat pipe alone 48.8 °C, demonstrating strong synergy in the hybrid configuration [69]. Comprehensive reviews of hybrid BTMS for EVs confirm that hybrid systems consistently outperform single-modality approaches across multiple performance indicators including maximum temperature, temperature uniformity, energy consumption, and thermal safety [70]. Honeycomb cold-plate hybrid systems optimised at 27 °C inlet temperature, 0.15 m/s inlet velocity, and 200 s reciprocating cycle period achieve T_max of 29.6 °C and ΔT of 2.0 °C [71].

3.4. Multi-criteria comparison

Experimental comparison of passive air cooling, indirect mini-channel liquid cooling (distilled water), lauric acid PCM, and hybrid ALC-PCM reveals that hybrid ALC-PCM achieves a temperature rise of only 3.5 °C at 40 °C ambient and 2 C discharge within the recommended 5 °C limit at an annual system cost of $61.8 with energy consumption of 0.0062% [72]. Fig. 7 presents a quantitative multi-criteria evaluation using spider diagram methodology across ten normalised performance indicators. Spider diagram comparing major BTMS categories (air cooling, liquid cooling, immersion cooling, passive PCM, heat pipe, hybrid PCM/liquid, hybrid PCM/heat pipe) across ten normalised performance indicators. Hybrid PCM/liquid exhibits the optimal profile with scores exceeding 9/10 for temperature control, uniformity, and fast-charge compatibility.

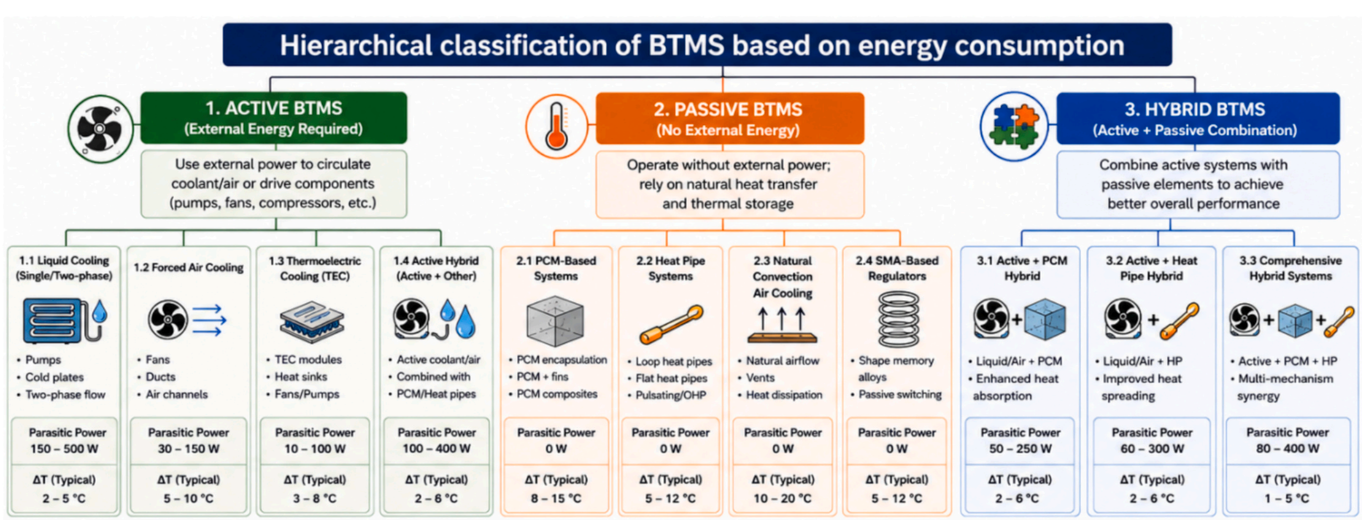

Fig. 6. Hierarchical classification of BTMS based on energy consumption.

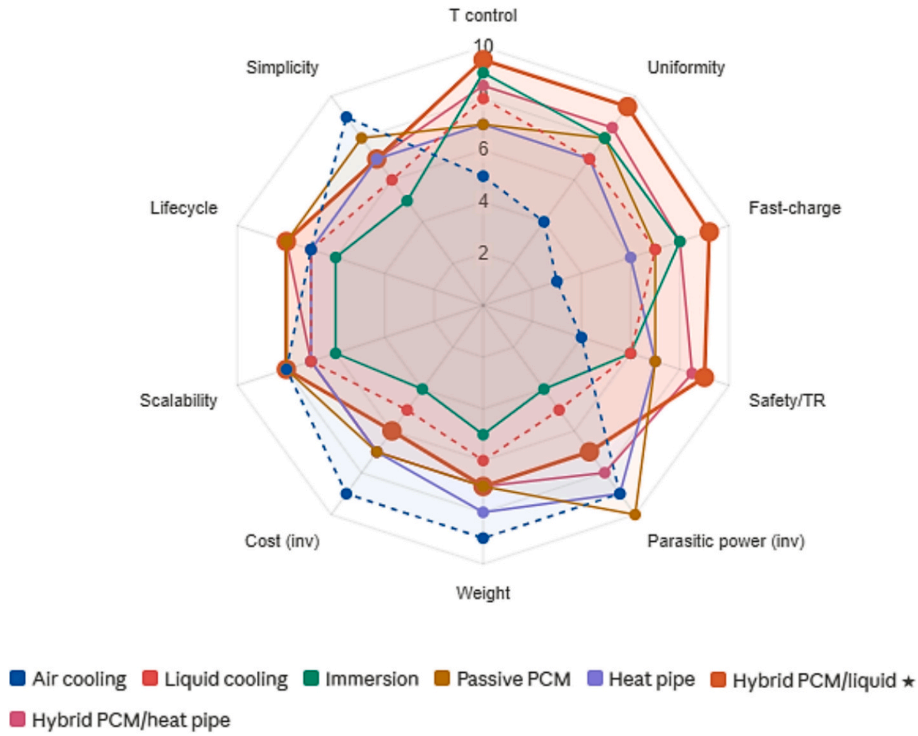

Fig. 7. Spider diagram comparing major BTMS categories (air cooling, liquid cooling, immersion cooling, passive PCM, heat pipe, hybrid PCM/liquid, hybrid PCM/heat pipe) across ten normalised performance indicators.

4. Phase change materials for BTMS: evolution and current challenges

4.1. Classification and thermophysical properties

PCMs suitable for EV BTMS are classified as organic (paraffins, fatty acids, polyethylene glycols), inorganic (salt hydrates, metallic alloys), and eutectic mixtures. Organic paraffins combine a tunable melting range of 30–60 °C with latent heats of 150–260 J g^{-1}, chemical stability, and low vapour pressure. Inorganic salt hydrates offer higher volumetric energy density but suffer from phase segregation, supercooling, and corrosivity [34]. Biodiesel-based PCMs represent an emerging class; palm biodiesel achieves 43% weight reduction compared to 3 M Novec while maintaining comparable cooling performance, reducing maximum LIB module temperature to 31.7 °C at 3 C discharge [73].

4.2. Leakage, low conductivity, supercooling, and volume expansion

Four persistent limitations impede widespread PCM deployment in BTMS: (i) low thermal conductivity (~0.2 W m^{-1} K^{-1}) restricting heat transfer rates; (ii) liquid-phase leakage causing contamination and electrical hazards; (iii) supercooling delaying heat release during battery preconditioning; and (iv) volume change (~10–15%) generating mechanical stresses in rigid modules [40]. A comprehensive review of PCM-based LIB BTMS covering advances, challenges, and future perspectives confirms these limitations as the primary barriers to commercial deployment and identifies nanocomposite engineering as the most promising mitigation pathway [74]. Advanced BTMS materials, cooling systems, and intelligent control strategies have been critically assessed, with materials advances particularly in composite PCMs identified as the highest-leverage research area for safety and performance improvement [75]. Sandwich-structured thermally conductive and insulating composite materials fabricated via electrospinning combined with hot-pressing achieve multiscale filler architecture capable of simultaneously enhancing through-plane conductivity and electrical insulation properties directly applicable to cell-level BTMS packaging [76]. Electrostatically engineered thermal interface materials with multiscale boron nitride–alumina–nanodiamond fillers achieve tailored anisotropic thermal conductivities in polyvinyl alcohol composites, demonstrating the potential of hierarchical filler architectures for directional heat management [77].

Graphite incorporation increases PCM thermal conductivity by up to 70 W m^{-1} K^{-1}; commercial passive systems utilising wax and graphite extend electric scooter driving range from 30 km to 55 km [78]. Sandwich-structured composites with boron nitride nanosheets (BNNS) and multi-walled carbon nanotubes (MWCNT) achieve in-plane thermal conductivity of 4.69 W m^{-1} K^{-1} at 14.75 wt% filler, approximately 23 times higher than the pure polymer matrix, while maintaining electrical insulation [76]. Critical review of polymer support-based shape-stabilised PCMs confirms that polymer matrix selection critically governs both mechanical integrity and leakage suppression, with cross-linked thermosets including epoxy resin demonstrating superior shape stability compared to thermoplastic supports [79]. Active and passive thermal management strategies exert distinct impacts on LIB aging trajectories; studies under constant and monthly average ambient temperature conditions confirm that passive PCM strategies reduce capacity-related aging penalties compared to purely active cooling at elevated ambient temperatures [80]. Supercooling mitigation primarily employs nucleating agents (carbon nanotubes, fine salt particles, nanoadditives), thickeners, and macroporous structures [81].

4.3. Shape-stabilisation strategies

Shape-stabilisation prevents PCM leakage without encapsulation shell overhead. Dual polymer-graphite nanoplatelet networks achieve radial thermal conductivities of 4.2–32.8 W m^{-1} K^{-1} at EG loadings of 5–40 wt% and reduce commercial LIB operating temperature by more than 12 °C at high discharge rates [82]. Form-stable PA/HDPE/EG/ER composites exhibit uniform structure and component compatibility, with PA thermal conductivity improving by a factor of 1.9 with only 6 wt

% EG addition [83]. Nanoporous structural EG/paraffin composites demonstrate that the nanoporous architecture of EG substantially improves PCM uptake capacity and effective thermal conductivity compared to conventional EG, producing robust shape-stabilised CPCMs with suppressed leakage and enhanced thermal performance applicable to LIB BTMS [84]. Review of phase change material use in EV battery thermal management confirms that EG loading at 10 wt% in paraffin-based composites achieves thermal conductivities of 9.99–10.70 W m^{-1} K^{-1} with latent heat of 231.67–240.06 J g^{-1}, residual mass exceeding 99% after 50 thermal cycles, and peak temperature reduction of 23 °C at 10 W heating power [78]. Fig. 8 illustrates the Pareto front of effective thermal conductivity versus latent heat for different PCM classes and EG/epoxy composites. Pristine organics cluster at high enthalpy/low k (~200 J g^{-1}, 0.2 W m^{-1} K^{-1}); nano-enhanced composites shift to $k > 15$ W m^{-1} K^{-1} with 10–30% enthalpy penalty; EG/epoxy formulations occupy the superior frontier with $k_{eff} = 10$–28 W m^{-1} K^{-1} and retained latent heat >170 J g^{-1}.

5. Expanded graphite as a high-performance conductive scaffold

5.1. Structural characteristics

Expanded graphite is produced by intercalation of graphite with strong acids followed by rapid thermal shock, generating a worm-like vermicular morphology with bulk density as low as 2–5 g L^{-1} and expansion volume up to 324 mL/g for sulfur-free preparations [2]. SEM, XRD, Raman, and TEM characterisation reveals that the microstructural integrity of graphite deteriorates upon infiltration with liquid paraffin, with interlayer spacing expanding. Thermal conductivity in the parallel direction reaches 20.8 W m^{-1} K^{-1} at 60 °C — approximately 70 times that of pure paraffin while conductivity in the normal direction remains substantially lower, producing pronounced anisotropy [85]. Fig. 9 illustrates the structural characteristics enabling EG's function as a thermal scaffold in composite PCMs. SEM images (Fig. 10) revealed that pure PA and LA possessed rough and uneven surface morphologies, whereas EG exhibited a worm-like porous reticulated structure with overlapping graphite layers and interconnected pores of varying sizes. These porous features enhanced the specific surface area and facilitated effective absorption of molten LA and PA within the EG matrix. The composite CPCM containing 15 wt% EG demonstrated nearly complete filling of EG pores by LA and PA, thereby minimizing leakage during phase transition. XRD analysis confirmed the presence of characteristic diffraction peaks corresponding to EG, PA, and LA without the formation of additional peaks, indicating that the composite formation occurred primarily through physical adsorption without significant structural or chemical changes [86].

5.2. Percolation network formation and optimal EG loading

The three-dimensional percolation network forms at 8–15 wt% EG loading. At 16–20 wt% EG, CPCMs achieve a shape-stabilised configuration with satisfactory thermal management performance; at 30 wt% EG, thermal conductivity reaches 13.85 W m^{-1} K^{-1} with a leakage ratio of only 0.38 wt% and the phase change temperature and latent heat remain close to those of the pure PCM (Fig. 11) [87]. Loadings of 5–30 wt% yield thermal conductivities of 2.671–10.019 W m^{-1} K^{-1} with phase transition enthalpies of 155.4–211.9 kJ/kg [87]. Composite PCMs with graphite nanosheets demonstrate that nanosheet morphology promotes more intimate interfacial contact than conventional EG particles, yielding higher thermal conductivity at equivalent filler loadings and providing complementary design options for battery thermal safety applications [88]. Fig. 11 shows the EG loading vs thermal conductivity and latent heat for PA/HD/EG/ER composite [Prepared from ref. 87].

6. Epoxy resin as structural and functional matrix in shape-stabilised CPCMS

Epoxy resin serves multiple synergistic roles in CPCMs: (i) structural binder that immobilises molten PCM and prevents leakage; (ii) mechanical reinforcement matrix improving compressive and tensile strength; (iii) electrical insulator maintaining dielectric isolation between cells; and (iv) fire-retardant char-former that synergises with the EG oxygen-blocking network. FT-IR analysis and flame tests confirm chemical integrity and self-extinguishing behaviour attributed to the oxygen-barrier effect of EG combined with ER char promotion yielding transient-only ignition and self-extinguishing under 30-s flame exposure

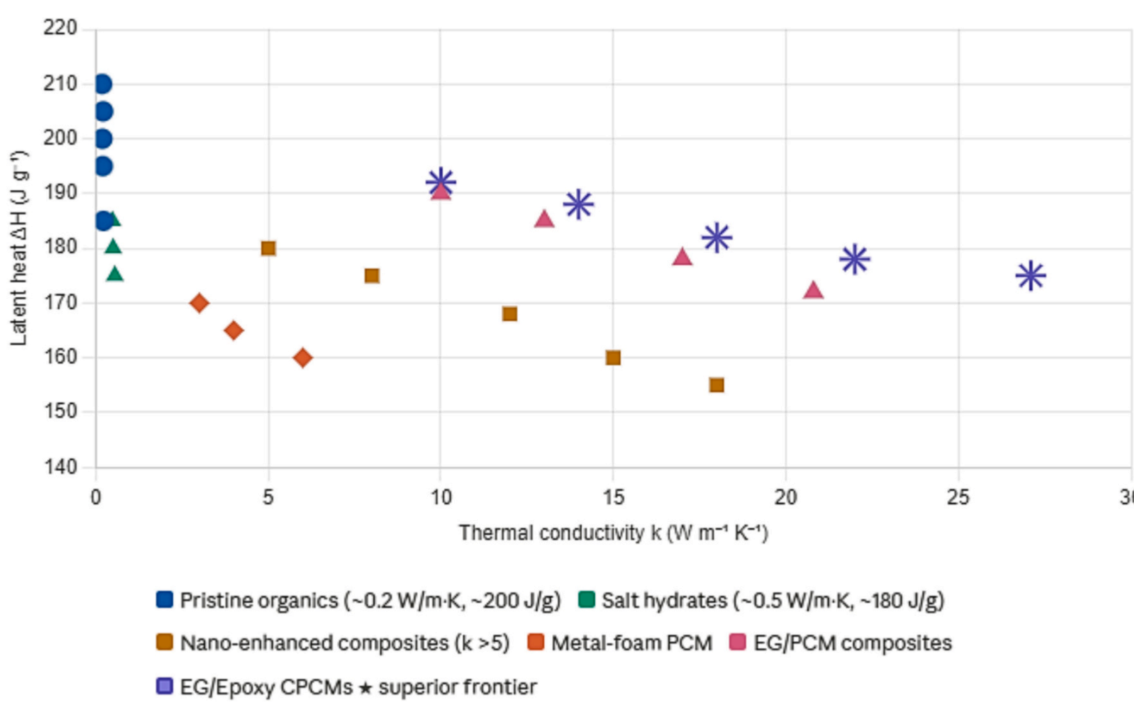

Fig. 8. Pareto front of effective thermal conductivity versus latent heat for different PCM classes.

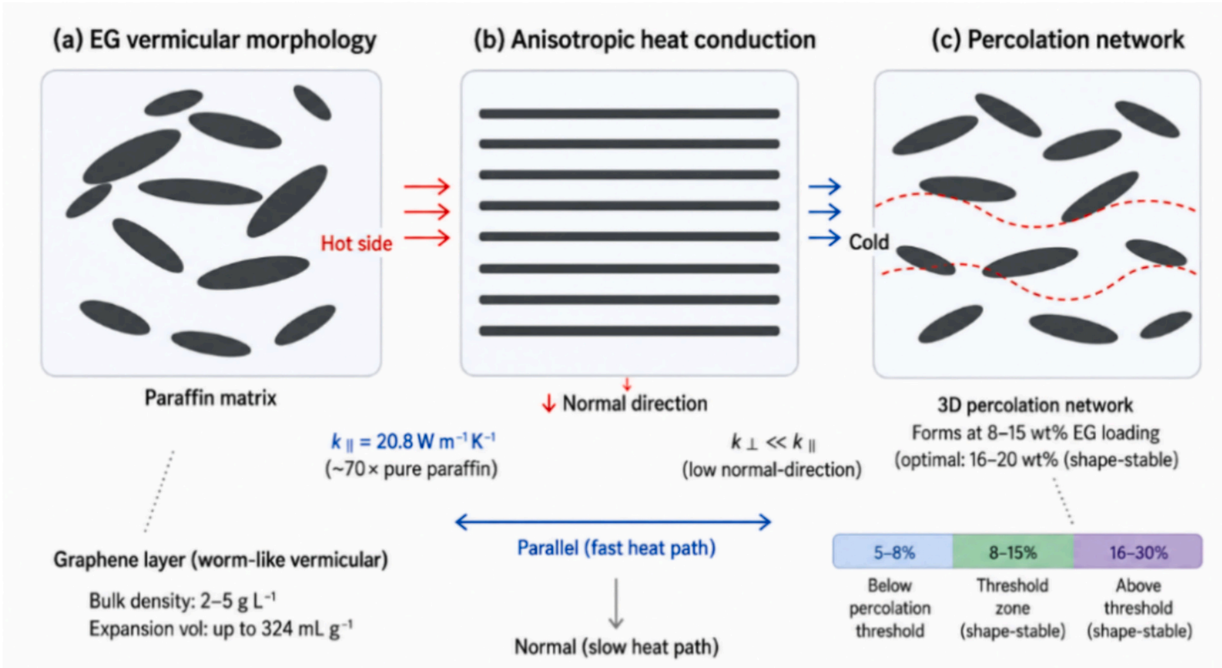

Fig. 9. Structural characteristics enabling EG's function as a thermal scaffold in composite PCMs.

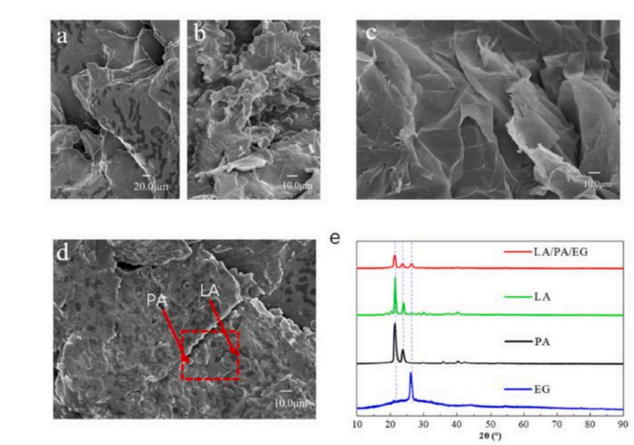

Fig. 10. Morphology of (a) PA, (b) LA, (c) EG; (d) LA/PA (1:1 in mass ratio) with 15 wt% EG; (e) XRD patterns of PA, LA, EG, and LA/PA (1:1 in mass ratio) with 15 wt% EG [86].

in 80/10/10 (PCM/EG/ER) composites [89]. Fig. 12 shows EG/epoxy CPCM integration in cylindrical and prismatic cell modules.

6.1. Mechanical and flame-retardancy properties

The ER/ATH/EG ternary composite (sample S5) demonstrates outstanding mechanical performance: 14.69% increase in compression strength and 400.12% increase in compression modulus compared to pure eutectic PCM, with thermal stability to 800 °C confirmed by thermogravimetric analysis (TGA) [4]. Notably, S5 exhibits enhanced thermal reliability during cycling: the initial latent heat of 150.4 J g^{-1} increases to 181.3 J g^{-1} after 100 heating–cooling cycles, confirming progressive microstructural densification and improved PCM–matrix compatibility [4]. The UL-94 V-0 classification – the highest flame-retardancy rating – is achieved through the collaborative synergy of ER, ATH, and EG, yielding 67.33% reduction in PHRR and 50.38% reduction in total heat release (THR) in cone calorimetry. The ternary composition also produces triple-layer PCM encapsulation from the synergistic ER/ATH interaction alongside the EG porous structure [4]. Introduction of flexible insulation networks into EG-based CPCMs simultaneously enhances dielectric properties and mechanical performance, enabling the material to serve as both a thermal barrier and an electrical insulator between adjacent cells [90]. Heat pipe/PCM coupled thermal management in Li-ion battery packs has been optimised for energy saving, with PCM-augmented heat pipe systems demonstrating lower annual energy consumption compared to active liquid cooling while maintaining acceptable temperature uniformity [91]. Myristic acid/EG composite PCMs prepared by melt impregnation achieve stable phase change behaviour over repeated thermal cycling, confirming chemical compatibility between fatty acid PCMs and graphite scaffolds relevant to long-term deployment [92]. Flame-retardant PCMs incorporating inorganic additives demonstrate improved fire performance metrics while maintaining sufficient latent heat for BTMS application, with battery module testing confirming the dual safety and thermal management functionality [93]. Enhanced BTMS designs integrating conventional heatsinks with thermoelectric modules and multi-layered PCMs demonstrate the benefit of stacked passive thermal buffers for extreme fast-charging scenarios, further substantiating the value of EG/epoxy CPCM layers in multi-material systems [94]. Fig. 13 illustrates the flame-retardancy mechanism for the EG/ER/ATH ternary composite, and Table 1 presents a comprehensive comparison of recent EG/epoxy CPCM formulations with their properties. Fig. 14 shows the benchmarking of EG/epoxy CPCMs versus other PCM composite systems. Radar chart comparing pristine PCM, EG/PCM composite, metal-foam PCM, microencapsulated PCM, and EG/epoxy CPCM across eight normalised performance criteria. EG/epoxy CPCM demonstrates highest aggregate scores for thermal conductivity, mechanical strength, flame retardancy, and cycling stability.

7. Synergistic EG/epoxy composite PCMS: state-of-the-art formulations

7.1. Optimal mass ratios and fabrication routes

Fabrication routes for EG/epoxy CPCMs include: (i) vacuum

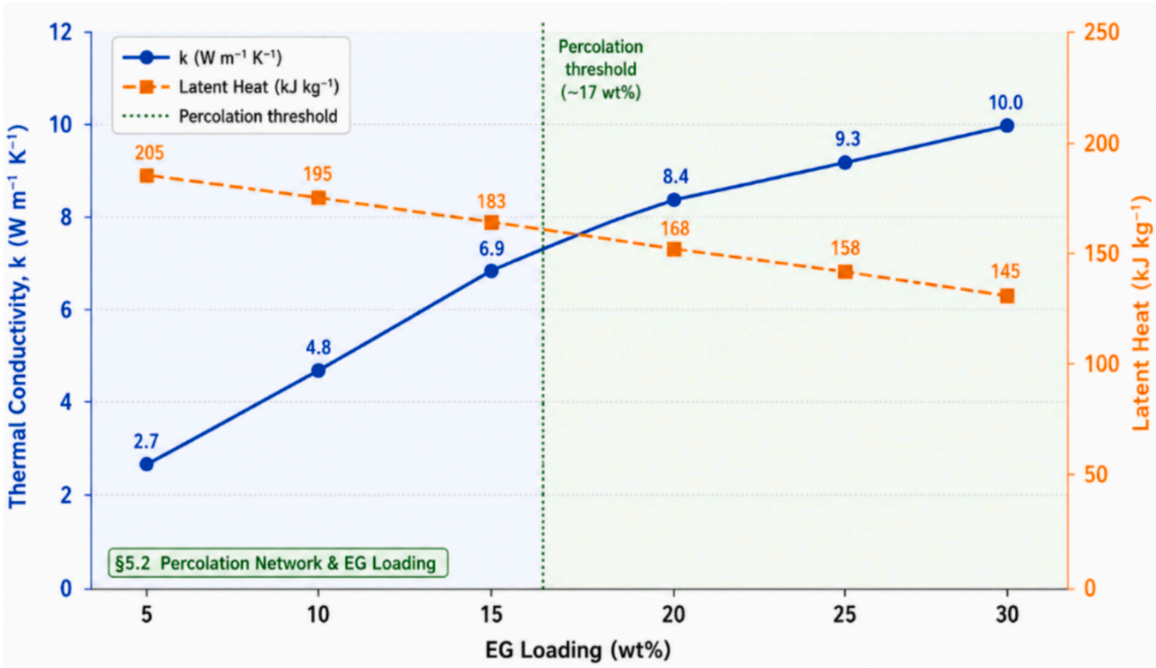

Fig. 11. EG loading vs thermal conductivity and latent heat for PA/HD/EG/ER composite.

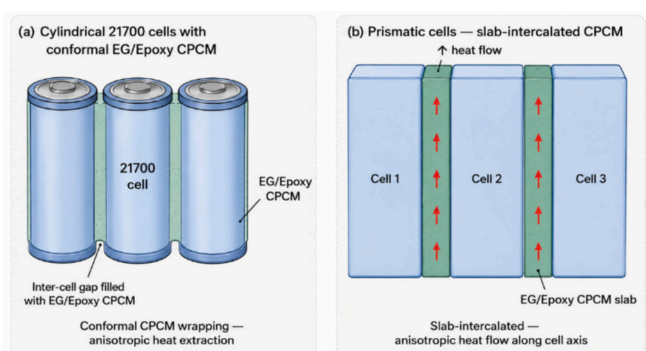

Fig. 12. EG/epoxy CPCM integration in cylindrical and prismatic cell modules. (a) Conformal EG/epoxy CPCM wrapping around 21,700 cylindrical cells. (b) Slab-intercalated CPCM layers in prismatic cell module showing anisotropic heat flow paths.

impregnation of PCM into the pre-formed EG porous scaffold; (ii) melt blending of PCM, EG, and epoxy resin followed by hot pressing for anisotropic EG orientation; (iii) in-situ polymerisation for enhanced interfacial bonding; and (iv) low-temperature solvent evaporation for improved dispersion and interfacial compatibility with reduced energy consumption [97]. The 80/10/10 (PCM/EG/ER) mass ratio represents an experimentally validated optimum that balances latent heat capacity, thermal conductivity, and mechanical integrity [89]. CPCMs with 16–20 wt% EG represent the most promising range for LIB thermal management, offering a shape-stabilised configuration with satisfactory performance across all key criteria [86]. Fig. 15 illustrates the principal fabrication routes and Table 2 compiles the highest reported values across key performance parameters for EG/epoxy CPCMs.

Among these, Reddy et al. [1] demonstrate thermal conductivity of 27.10 W m^{-1} K^{-1} exceeding pure paraffin (0.24 W m^{-1} K^{-1}) by two orders of magnitude with compressive and tensile strengths of 39.4 MPa and 9.0 MPa, maintaining battery surface temperatures below 42 °C versus >52 °C for conventional systems. Luo et al. [3] achieve maximum battery temperature of 33 °C with $\Delta T = 1.4$ °C at 4 C discharge, and 44.8 °C after six extreme cycles, using dual-phase PCM combined with EG ($k = 40$ W m^{-1} K^{-1}) and epoxy resin in 5:2:3 mass ratio with graphite film (in-plane $k = 1400$ W m^{-1} K^{-1}). The Fig. 16 shows benchmarking of top EG/epoxy CPCMs against other composite PCM systems on eight normalised criteria. EG/epoxy systems achieve aggregate scores >85/100 with conductivity >20 W m^{-1} K^{-1}, enthalpy >170 J g^{-1}, and compressive strength >8 MPa.

8. Experimental and numerical characterisation techniques

8.1. Thermal conductivity measurement

Laser flash analysis (LFA) is the primary technique for measuring through-plane and in-plane thermal diffusivity, from which conductivity is calculated using independently measured density and specific heat capacity. Thermal conductivity in the parallel direction of EG/paraffin composites reaches 20.8 W m^{-1} K^{-1} at 60 °C [85]. An anisotropy degree derived from SEM morphology quantitatively describes the graphite sheet distribution evolution within the paraffin matrix. Comparative LFA measurements on PW/EG composites show that the pressure-induced method achieves 9.99 W m^{-1} K^{-1} with latent heat 240.06 J g^{-1}, versus 10.70 W m^{-1} K^{-1} with latent heat 231.67 J g^{-1} for the prefabricated skeleton method at 10 wt% EG [84].

8.2. Thermal analysis and mechanical testing

Differential scanning calorimetry (DSC) at 5–10 °C min^{-1} characterises phase change onset, peak, and enthalpy. DSC measurements on EG/PA-5.0 composites demonstrate latent heat of 253.08 J g^{-1} [2]. TGA confirms thermal stability of ER/ATH/EG composites up to 800 °C [4]. Leakage testing by isothermal hold at 70 °C with mass measurement confirms residual mass fractions exceeding 99% after 50 thermal cycles [84]. Mechanical testing per ASTM D695 demonstrates compressive strength of 39.4 MPa and tensile strength of 9.0 MPa for EG-enhanced composites [1]. The ER/ATH/EG composite shows 14.69% increase in compression strength and 400.12% increase in compression modulus compared to pure eutectic PCM [4]. Cone calorimetry (ISO 5660) characterises fire performance through PHRR, THR, and time-to-

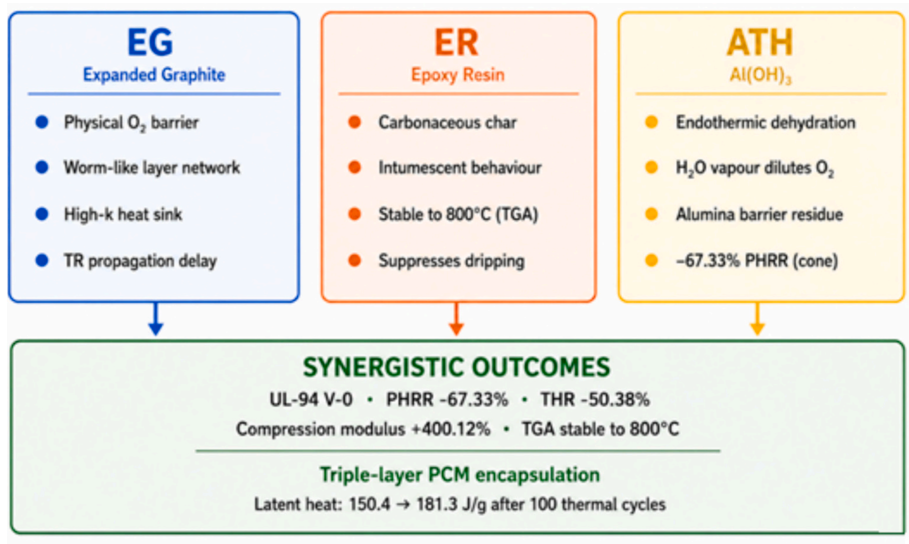

Fig. 13. Flame-retardancy mechanism for EG/ER/ATH ternary composite.

ignition measurements.

8.3. Module-level experimental validation

Module-level testing integrates CPCM-wrapped cells in representative configurations. Integration of 80/10/10 SSPCM into cylindrical 18,650 cells in a 2S2P battery pack configuration maintains surface temperatures at 37.2 °C under 2 C discharge and 50.5 °C under 4 C discharge, with peak temperature reduction of 40% relative to air cooling and additional reductions of 16.8% and 33.1% compared to pure PCM and silicone oil, respectively [89]. Thermomagnetic oscillator cooling systems offer hybrid waste heat recovery and direct cooling in a single compact device, representing an emerging active BTMS modality applicable to EV thermal architecture [98]. Immersion cooling control strategies for unevenly degraded LIB cells under fast-charging demonstrate that adaptive feedback control maintains more uniform cell temperatures than fixed flow-rate approaches [99]. A novel PCM/EG composite sphere with high thermal conductivity and excellent shape stability demonstrates suitability for packed-bed thermal energy storage systems, extending EG/PCM composite applications beyond flat-plate BTMS geometries [100]. All-climate thermal management structures based on EG/polymer composite PCMs achieve high thermal and electrical conductivity simultaneously, enabling year-round operation across both high-temperature cooling and low-temperature pre-heating scenarios [101]. High thermal conductivity anti-leakage CPCMs incorporating halloysite nanotubes within EG matrices demonstrate improved thermal conductivity, mechanical strength, and leakage resistance relevant to BTMS application [102]. Pin fin heat sinks integrated with PCMs for electronic device thermal management confirm that combined conduction-enhancement and latent-heat-storage approaches outperform either strategy alone, informing EG/epoxy CPCM design for high-power density applications [103]. Hydrated salt/modified EG-based form-stable CPCMs demonstrate high latent heat and stable phase change characteristics relevant to non-automotive thermal energy storage applications, expanding the knowledge base for EG composite design [104]. Phase change materials encapsulated in hybrid carbon skeletons combining graphene and carbon nanotube networks achieve simultaneous high solar-thermal conversion efficiency and latent heat storage, providing insights into multi-functional carbon scaffold architectures [105]. A Z-type cold plate/PCM composite hybrid liquid cooling system achieves compact and lightweight thermal management for battery modules, with EG-enhanced PCM contributing to uniform temperature distribution across cells [106]. Water immersion cooling for cylindrical battery cells demonstrates that direct liquid contact substantially reduces maximum temperature under high discharge rates, contextualising the role of passive CPCMs in hybrid architectures [107]. Coupled electrochemical-thermal modelling of Li-ion battery pack thermal management systems provides validated simulation frameworks applicable to EG/epoxy CPCM-integrated pack design [108]. Performance evaluation of liquid-PCM hybrid BTMS with spatial network flow channels demonstrates that optimised channel geometry significantly reduces both maximum temperature and temperature non-uniformity, outperforming conventional parallel-plate configurations [109]. Multi-objective topology optimisation of nanofluid cooling plates for LIB pack thermal management provides a computational framework for maximising temperature uniformity with minimum coolant pumping power [110]. Anisotropic flexible PCMs for cylindrical battery thermal management demonstrate that directional thermal conductivity aligned with the cell axis significantly improves heat extraction efficiency compared to isotropic CPCMs [111].

8.4. Multi-physics modelling

Pseudo-two-dimensional electrochemical-thermal models implemented in COMSOL Multiphysics quantify temperature distributions, crystallographic strain, and electrolyte decomposition effects, with model validation yielding RMSE of 0.08 at 0.15 C discharge [46]. Three-dimensional COMSOL simulations calibrated with experimental data establish quantitative thermal design criteria for TR suppression [58]. AI-driven approaches using machine learning techniques and physics-informed neural networks are emerging as transformative tools for real-time BTMS prediction and multi-objective optimisation [112]. Fig. 17 presents representative multi-physics modelling: (a) experimental LFA configuration and (b) numerical CFD domain for EG/Epoxy CPCM-based BTMS.

9. System-level integration and real-world performance

Under extreme fast charging (4 C), the dual-phase PCM + EG + ER + graphite film system maintains maximum battery temperature at 33 °C with $\Delta T = 1.4$ °C, and a maximum of only 44.8 °C after six consecutive extreme cycles [3]. CPCM cooling maintains maximum battery temperature below 43 °C with ΔT of 1.96 °C, cooling stability of 83.5%, and negligible capacity loss of 0.0016% per cycle [86]. These performance levels satisfy or exceed all principal thermal design criteria listed in Section 2.4. Table 3 summarises quantitative TR suppression

Table 1
Comprehensive comparison of recent EG/epoxy CPCM formulations (2019–2025).

Ref.	Authors (year)	PCM base	EG wt %	Additives	k (W m^{-1} K^{-1})	Latent heat (J g^{-1})	T_melt (°C)	T_max battery (°C)	Key findings
[1]	Reddy et al. (2025)	Paraffin wax	20	None	27.10	–	~45–52	<42	Highest reported k for EG/PCM CPCM; compressive strength 39.4 MPa, tensile 9.0 MPa; battery T < 42 °C vs. >52 °C baseline
[2]	Zhang et al. (2025)	Paraffin (EG/PA)	–	Sulfur-free EG	High	253.08	~50–55	–	Sulfur-free EG; expansion volume 324 mL/g; highest latent heat reported for EG/paraffin CPCM
[3]	Luo et al. (2019)	Dual-phase PCM	–	Graphite film (1400 W/m·K)	40 (EG)	–	–	33	T_max = 33 °C, ΔT = 1.4 °C at 4 C; 44.8 °C after 6 extreme cycles; EG:ER: PCM = 5:2:3
[4]	Pea et al. (2024)	OA/OL eutectic	10	Epoxy resin, ATH	–	150.4 → 181.3	~50	–	UL-94 V-0; PHRR −67.33%, THR −50.38%; compression modulus + 400.12%; TGA stable to 800 °C
[82]	Xu (2020)	Polymer/GNP	16–20	Graphite nanoplatelets	4.2–32.8	–	–	−12 °C	Dual polymer-GNP network; k = 4.2–32.8 W/m·K at 5–40 wt%; reduces LIB T by >12 °C
[83]	Pea et al. (2023)	Paraffin/HDPE	6	HDPE, Epoxy resin	1.9× pure PA	–	–	–	PA thermal conductivity ×1.9 with 6 wt % EG; form-stable PA/HDPE/EG/ER composite
[84]	Zhao et al. (2025)	Paraffin wax (PW)	–	Nanoporous EG	9.99–10.70	231.67–240.06	–	–	Nanoporous EG structure enhances PCM uptake and thermal conductivity vs. conventional EG; shape-stabilised; lower leakage
[85]	Wang et al. (2020)	Paraffin (EG/paraffin)	–	None	20.8 (‖)	–	60	–	Parallel-direction k = 20.8 W/m·K at 60 °C; pronounced thermal anisotropy characterised
[86]	Zhang et al. (2023)	Lauric acid–paraffin	–	Expanded graphite	–	–	–	–	Low-cost LA–paraffin–EG CPCM; quenches TR of LIBs; multifunctional composite
[87]	Lin et al. (2021)	Polymer/EG	–	Polymer matrix	–	–	–	–	Flexible EG/polymer CPCM; high thermal conductivity; suitable for battery thermal management
[89]	Hyun et al. (2025)	Organic PCM	–	Epoxy resin, EG	–	–	–	–	Flame-retardant shape-stabilised PCM; enhanced safety for high-power LIBs
[90]	Yang et al. (2023)	Paraffin	20	Anisotropy EG	High	–	–	–	High anti-leakage; anisotropic EG enhances directional conductivity for battery thermal management
[92]	Zhou et al. (2020)	Myristic acid	–	Expanded graphite	–	–	–	<44.7	PSTE4: T_max < 44.7 °C, ΔT < 3.6 °C; anti-leakage >99.9% at 70 °C
[93]	Cui et al. (2023)	Lauric acid–paraffin	–	Expanded graphite	–	–	–	<43	T_max < 43 °C, ΔT = 1.96 °C; cooling stability 83.5%; capacity loss 0.0016%/cycle
[95]	Yang et al. (2023)	EG-based	–	Flexible insulation net	–	–	–	–	Flexible insulation network; enhanced dielectric + mechanical properties; dual thermal/electrical barrier
[97]	Marri et al. (2025)	Composite PCM	–	Epoxy resin	–	–	–	–	High-performance moldable CPCM; scalable external thermoregulation of Li-ion batteries
[101]	Cheng et al. (2022)	EG/polymer	–	Polymer matrix	–	–	–	–	All-climate structure; high thermal + electrical conductivity; year-round heating/cooling
[102]	Yang et al. (2023)	EG-based	–	Halloysite nanotubes	–	–	–	–	Anti-leakage CPCM with HNT; improved k, mechanical strength, leakage resistance
[104]	Pea et al. (2023)	Paraffin/HDPE	5–30	HDPE, epoxy resin	2.671–10.019	155.4–211.9 kJ/kg	–	–	5–30 wt% EG; k = 2.671–10.019 W/m·K; enthalpy 155.4–211.9 kJ/kg
[121]	Zhao et al. (2025)	Metal alloy/EG/paraffin	–	Metal alloy	–	–	–	–	All-season applicability; wide melting-point tunability; combined cooling + pre-heating

performance data for EG/epoxy CPCMs drawn from module-level and cell-level experimental studies.

The ternary ER/ATH/EG composition yields 67.33% reduction in PHRR and 50.38% reduction in THR with UL-94 V-0 classification, establishing a robust defence against rapid flame propagation [4]. The integrated liquid channel/aerogel structure mitigates TR propagation at a mass flow rate 7-fold lower than conventional single liquid cooling plates [55]. Fig. 18 presents a comparative spider diagram for hybrid BTMS performance where EG/epoxy PCM plus liquid cooling achieves highest overall score exceeding 92/100 across ten normalised metrics.

10. Sustainability, cost and industrial scalability

10.1. Life-cycle assessment and SDG alignment

EV adoption positively impacts 40 Sustainable Development Goals (SDGs) while negatively affecting 5 [113]. EG/epoxy CPCMs directly support SDG 7 (Affordable and Clean Energy) through lightweight, low-parasitic thermal management that reduces traction energy consumption, and SDG 11 (Sustainable Cities and Communities) through enhanced safety and reduced battery failure rates. The transition from

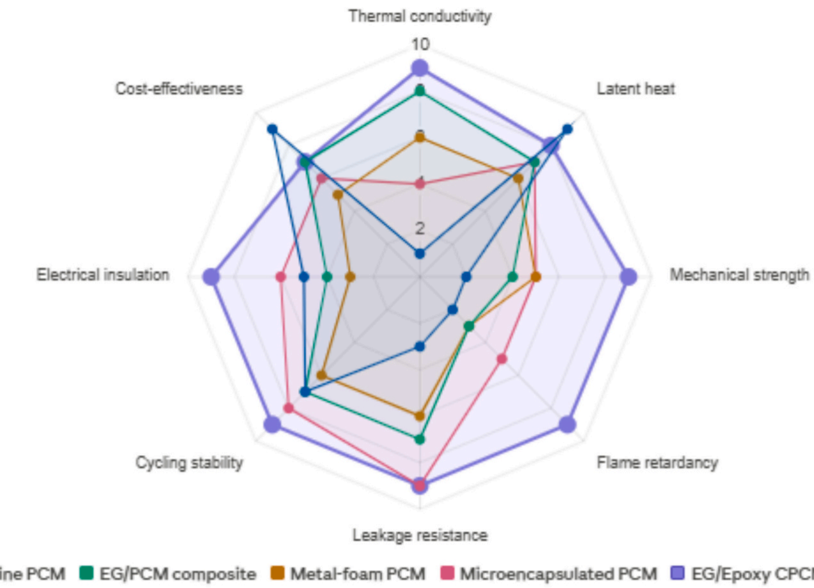

Fig. 14. Radar chart comparing pristine PCM, EG/PCM composite, metal-foam PCM, microencapsulated PCM, and EG/epoxy CPCM across eight normalised performance criteria.

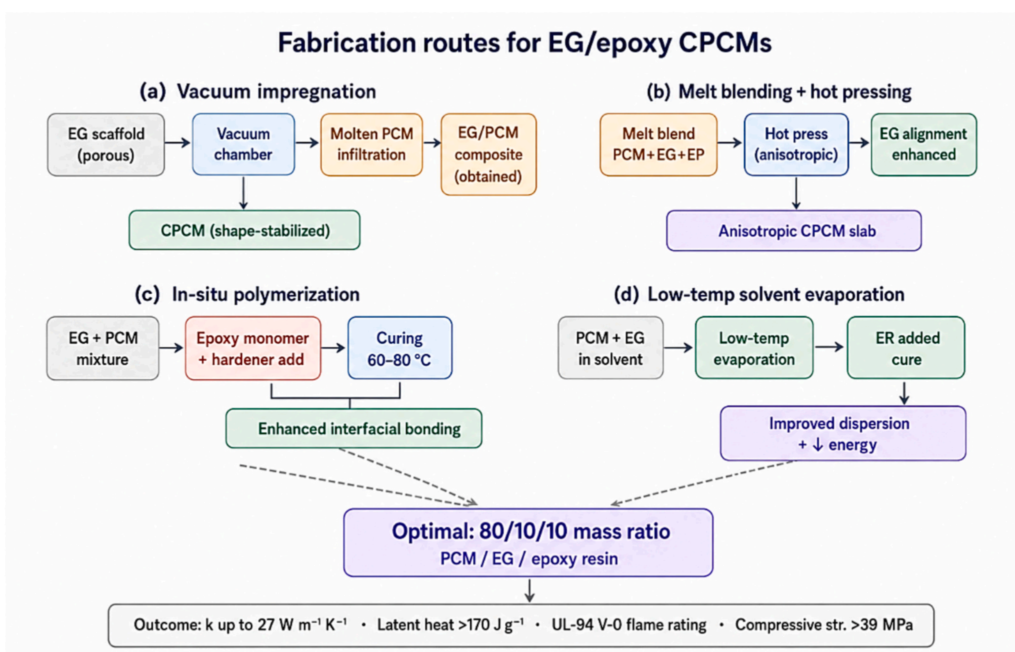

Fig. 15. Fabrication routes for EG/epoxy CPCMs: (a) vacuum impregnation of PCM into EG porous scaffold; (b) melt blending with hot pressing for anisotropic EG orientation; (c) in-situ polymerisation for enhanced interfacial bonding; (d) low-temperature solvent evaporation.

internal combustion engine vehicles to EVs in the UK, while requiring an additional 81 TWh of electricity annually, is projected to reduce total national CO_2 emissions by approximately 12%, with net environmental benefits increasing as grid decarbonisation progresses [114]. Environmental policy stringency restricting trade in coal, petroleum, and natural gas is a key macroeconomic lever driving the shift toward clean energy sources, creating the regulatory backdrop for accelerating EV market growth [115]. EV societal, environmental, and economic impacts assessed against the SDG framework confirm that emissions reduction, resource efficiency, and urban air quality improvement are the dominant positive contributions of electrification [113]. Air quality monitoring during commuting by various transport modes confirms that EVs significantly reduce passenger exposure to NO_2 and particulate matter compared to internal combustion engine vehicles, directly supporting SDG 3 (Good Health and Well-being) [116]. Global clean energy investment increased by 17% to $1.7 trillion in 2023, with renewable capacity projected to grow from 4250 GW to nearly 10,000 GW by 2030 [117]. A system dynamic sustainability assessment model for urban energy transition demonstrates that EV fleet electrification is a critical lever for achieving net-zero urban energy targets [118].

Assessment of hybrid EV futures in the UK confirms that plug-in hybrid and fully electric powertrains contribute substantially to transport decarbonisation when combined with renewable electricity generation [119]. Energy demand time series generation methods for energy system modelling underpin the analytical framework used to estimate BTMS energy consumption impact at fleet scale [120]. Metal

Table 2
Record-performing EG/epoxy CPCM systems.

Ref	Authors (year)	Composition	k (W m^{-1} K^{-1})	Latent heat (J g^{-1})	Comp. strength (MPa)	Tensile strength (MPa)	T_max battery (°C)	Record/standout achievement
[1]	Reddy et al. (2025)	EG/paraffin wax CPCM	27.10	–	39.4	9.0	<42	Highest k reported (27.10 W/m·K); compressive 39.4 MPa; tensile 9.0 MPa; battery $T < 42$ °C vs. >52 °C baseline
[2]	Zhang et al. (2025)	Sulfur-free EG/paraffin CPCM	High	253.08	–	–	–	Highest latent heat (253.08 J g^{-1}) for EG/paraffin; expansion volume 324 mL/g; sulfur-free process
[3]	Luo et al. (2019)	Dual-PCM + EG + ER + graphite film	40 (EG)	–	–	–	33	Lowest T_max (33 °C) + ΔT = 1.4 °C at 4 C discharge; 44.8 °C after 6 extreme cycles; graphite film k = 1400 W/m·K
[4]	Pea et al. (2024)	OA/OL/EG/ER/ATH (80/10/5/5 wt%)	–	150.4 → 181.3	–	–	–	UL-94 V-0 (highest flame class); PHRR −67.33%; THR −50.38%; compression modulus +400.12%
[82]	Xu (2020)	Polymer/GNP dual-network	4.2–32.8	–	–	–	−12 °C	Radial k up to 32.8 W/m·K at 40 wt%; reduces LIB T by >12 °C at high discharge
[84]	Zhao et al. (2025)	Paraffin/nanoporous EG	Enhanced	–	–	–	–	Nanoporous EG scaffold enhances PCM uptake and thermal conductivity; superior shape-stabilisation vs. conventional EG
[85]	Wang et al. (2020)	EG/paraffin (parallel direction)	20.8	–	–	–	–	Parallel-direction k = 20.8 W/m·K at 60 °C (~70× pure paraffin); pronounced anisotropy characterised
[92]	Zhou et al. (2020)	Myristic acid/EG CPCM (PSTE4)	–	–	–	–	<44.7	T_max <44.7 °C; ΔT < 3.6 °C; anti-leakage >99.9% at 70 °C; stable thermal cycling
[93]	Cui et al. (2023)	LA–paraffin–EG CPCM	–	–	–	–	< 43	T_max < 43 °C; ΔT = 1.96 °C; cooling stability 83.5%; capacity loss 0.0016%/cycle
[104]	Pea et al. (2023)	OA/OL eutectic 80/10/10 Shape-stabilised phase change material (SSPCM)	–	150.4	–	–	37.2/50.5	2S2P 18,650 pack; 37.2°C at 2 C/50.5 °C at 4 C; peak T reduction −40% vs. air; −16.8% vs. pure PCM

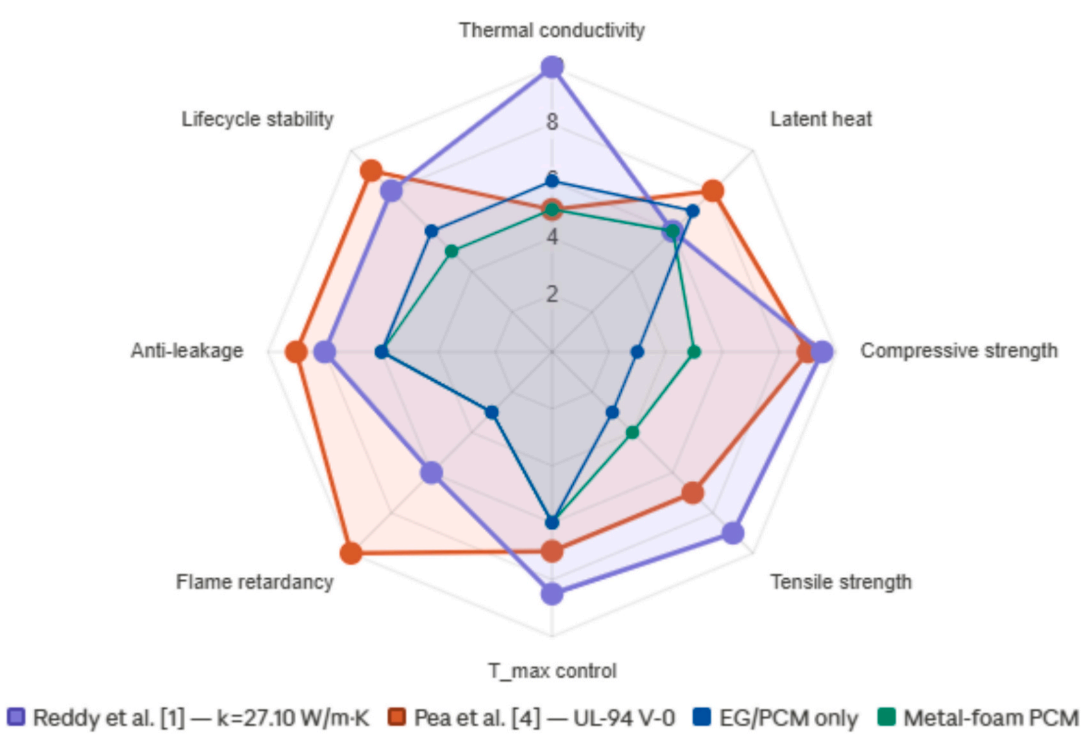

Fig. 16. Benchmarking of top EG/epoxy CPCMs against other composite PCM systems on eight normalised criteria.

alloy/EG/paraffin composite PCMs demonstrate all-season applicability through wide-range melting point tunability, confirming that EG-based composites can be designed for both cooling and pre-heating functions within a single material system [121]. Waste heat recovery applications of PCMs including industrial process heat capture and re-use highlight the broader economic and sustainability case for advanced composite PCM adoption beyond battery thermal management [122]. Deep potential molecular dynamics simulations of molten salt systems across phase transition temperatures provide atomistic-level insights into phonon transport mechanisms applicable to computational optimisation of inorganic PCM formulations [123]. Fig. 19 presents the SDG contribution mapping.

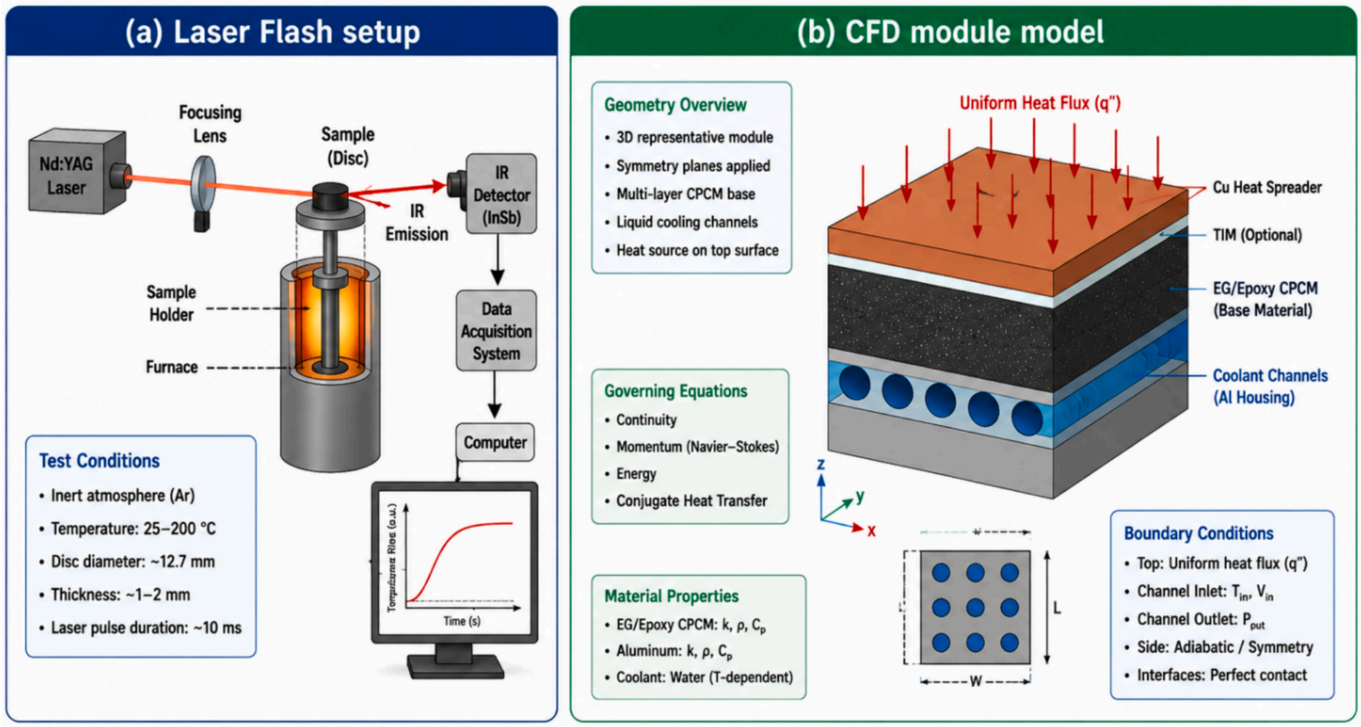

Fig. 17. Representative multi-physics modelling (a) Experimental LFA configuration and (b) numerical CFD domain for EG/Epoxy CPCM-based BTMS.

10.2. Manufacturing cost and gigafactory readiness

Cost drivers for EG/epoxy CPCMs include: EG raw material (intercalation acid cost reduced by sulfur-free routes [2]), epoxy resin grade, and processing energy. Low-temperature solvent evaporation fabrication techniques significantly reduce energy consumption during synthesis while ensuring improved dispersion, interfacial compatibility, and structural integrity [97]. The scalability of melt blending and hot-pressing routes is compatible with existing battery pack assembly lines at gigafactory scale, with CPCMs in the 16–20 wt% EG range representing the most cost-effective configuration [96]. Reformulation of ceramic body compositions demonstrates that optimising material constituents can simultaneously improve thermal efficiency and reduce manufacturing energy consumption, a principle directly applicable to EG/epoxy CPCM production scale-up [124]. Distributed activation energy models for polymer waste thermal decomposition provide kinetic frameworks applicable to safety assessment of paraffin-based CPCM components under potential fire exposure conditions [125]. Building information modelling integrated with augmented reality for energy systems visualisation provides digital twin methodologies applicable to BTMS system-level design and predictive maintenance [126]. Coupled electrochemical-thermal modelling validated against battery pack data establishes physics-based design criteria for BTMS optimisation that complement experimental characterisation of EG/epoxy CPCMs [108]. Energy management and control advances in direct current microgrids for smart cities are enabling the intelligent EV charging infrastructure that will demand high-performance BTMS to manage increased thermal loads from fast charging [127]. Generic frameworks for distributed multi-generation and multi-storage energy systems contextualise battery pack thermal management within broader energy network architectures relevant to vehicle-to-grid applications [128]. Non-uniform internal heat source modelling in PCM/water cooling-plate BTMS demonstrates that accounting for spatial heat generation heterogeneity is essential for accurate thermal performance prediction in multi-cell modules [129]. Transient thermal analysis of passive air-cooled battery packs across various casing materials identifies thermal conductivity and specific heat capacity of the casing as key parameters governing peak temperature under high-rate discharge [130]. Experimental and numerical investigation of hybrid BTMS for electric vans confirms that combining PCM with liquid cooling delivers both improved temperature uniformity and reduced energy consumption compared to liquid-only cooling under real-world duty cycles [131]. Lumped diffusion models for LIB voltage prediction under dynamic loads demonstrate that accurate electrochemical-thermal coupling requires appropriate diffusion representations, providing model selection guidance for BTMS simulation frameworks [132].

11. Challenges, research gaps and future directions

11.1. Remaining technical barriers

Despite advances, several barriers inhibit full deployment of EG/epoxy CPCMs in production EV packs:

- Thermal conductivity below 5 W m^{-1} K^{-1} in the through-plane direction for many formulations, limiting heat extraction to liquid cooling channels.
- Long-term cycling stability beyond 500 cycles under combined thermal-mechanical loading remains inadequately characterised.
- Volume change accommodation under pack-level constraint forces requires validated structural models.
- Flammability of paraffin-based PCMs necessitates flame-retardant additives that may reduce latent heat [40,43]. Flexible flame-retardant CPCMs with styrene block copolymer elastic networks demonstrate that aging-induced latent heat degradation can be substantially mitigated compared to rigid CPCM formulations, with the aged PAPS/EG composite retaining UL-94 V-0 rating after 200 thermal cycles providing a design blueprint for long-term stable flame-retardant EG/epoxy CPCMs [133]. Liquid BTMS combining heat dissipation and pre-heating functions in a single structure demonstrate that a pipe diameter of 10 mm with a flow rate of 0.02 m/s achieves optimal heat transfer intensity, informing the hydraulic

Table 3
Thermal runaway suppression performance of EG/epoxy CPCMs compared to baseline conditions.

Ref	Authors (year)	Material system	Test condition	PHRR reduction	THR reduction	Flame rating	TR propagation effect	Key TR suppression results
[4]	Pea et al. (2024)	OA/OL/EG/ER/ATH ternary CPCM	Cone calorimetry (ISO 5660)	−67.33%	−50.38%	UL-94 V-0	–	Highest combined flame suppression; compression modulus +400.12%; TGA stable to 800 °C; triple-layer PCM encapsulation
[32]	Hu et al. (2022)	LIB module under charging (3 C vs 0.5 C)	Overcharge TR propagation	–	–	–	12.1% at 3 C vs. 0.5 C	TR propagation time at 3 C = 12.1% of that at 0.5 C; lowest onset T = 127.4 °C; air-mediated heat conduction = 67% of inter-cell transfer
[53]	Novotny et al. (2025)	Prismatic NMC811 (156 Ah)	Cyclone-Calorimetry TR evaluation	–	–	–	–	TR energy release 2.5–2.9 MJ; 31–40% retained in cell; 60–69% vented; 55–63% ejected particles (≥88% by mass ≤ 1 mm diameter)
[55]	Lyu et al. (2025)	Integrated liquid channel + aerogel	TR propagation test (prismatic)	–	–	–	7× lower flow rate	TR mitigated at 4×10^{-6} kg/s (7-fold lower than single cooling plate 2.8×10^{-5} kg/s); aerogel ↑ suppresses heat transfer ratio from 66% to 44%
[58]	Liu et al. (2025)	Thermal barrier (3-D COMSOL simulation)	TR propagation simulation	–	–	–	+26% delay	Cp increase of 60% delays TR propagation by ~26%; anisotropic k raises suppression threshold by ~28% vs. isotropic barrier
[86]	Zhang et al. (2023)	LA–paraffin–EG CPCM	LIB TR quench test	–	–	–	–	Quenches LIB TR; low-cost multifunctional CPCM; EG enhances k and suppresses combustion propagation
[89]	Hyun et al. (2025)	Organic PCM/Epoxy resin/EG shape-stabilised	High-power LIB safety test	–	–	V-0 equivalent	–	Flame-retardant shape-stabilised PCM; thermally conductive; enhanced safety for high-power LIBs
[90]	Yang et al. (2023)	EG-CPCM + flexible insulation network	Dielectric + mechanical tests	–	–	–	–	Flexible insulation network; enhanced dielectric properties; serves as thermal barrier + electrical insulator between cells
[93]	Cui et al. (2023)	LA–paraffin–EG flame-retardant CPCM	Battery module TR protection test	Significant	Significant	Improved	–	Dual flame-retardancy + thermal management; module T_max < 43 °C; capacity loss only 0.0016%/cycle; ΔT = 1.96 °C
[104]	Pea et al. (2024)	OA/OL eutectic 80/10/10 SSPCM in 18,650 pack	Module-level 2S2P pack test	–	–	Self-extinguish	–	Transient-only ignition under 30-s flame; self-extinguishing behaviour; UL-94 V-0; EG + ER oxygen-barrier synergy
[133]	Deng et al. (2023)	Flexible flame-retardant CPCM (PAPS/EG)	200 thermal aging cycles test	–	–	V-0 retained	–	After 200 thermal cycles aged PAPS/EG retains UL-94 V-0; LOI = 30.1%; latent heat decreases from 118 to 102 J g^{-1} only; T_max = 46.5 °C, ΔT = 3.5 °C at 3 C

design of hybrid EG/epoxy CPCM/liquid cooling systems [134]. Wavelet transform analysis of compressed air system pressure signals offers a methodology for pattern-based event detection applicable to BTMS anomaly monitoring and fault diagnosis [135]. EG/CPCM coupled with water cooling in double S-shaped micro-channels achieves superior heat dissipation compared to passive CPCM alone at 3 C discharge and 40 °C ambient, with 20 wt% EG identified as the optimal loading for maximum cooling effectiveness [136]. Series-connected $LiFePO_4$ battery pack thermal and electrical performance under liquid cooling at multiple discharge rates confirms that coolant temperature of 30 °C provides the optimal balance between temperature uniformity and discharge capacity [137]. Long-term structural vibration monitoring of reinforced concrete structures under temperature and humidity variation provides methodological insights into combined thermal-mechanical loading characterisation applicable to EG/epoxy CPCM durability testing under vehicle operating conditions [138]. Fig. 20 highlights the various challenges, research gaps and future directions in BTMS for LIB technology.

11.2. Flexible and wearable CPCMs for solid-state batteries

Next-generation solid-state batteries require conformable thermal management materials. Novel NXPCMs with linear polymer architectures achieve tensile strength of 15.83 MPa and elongation at break of 949.8%, with phase change temperature tuneable between 40.1 °C and 50.9 °C via polyethylene glycol segment length, and latent heat of 93.89–131.3 J g^{-1} [139]. Ultra-flexible multifunctional CPCMs using olefin block copolymer, SEBS, PDMS, CNTs, and carbon cloth achieve 240.2% elongation with latent heat of 155.4 J g^{-1}, reducing maximum battery temperature by 21.7 °C during overheating and increasing discharge time by 53.1% at low temperatures [140]. Fig. 21 shows the next-generation flexible CPCM properties in a solid-state battery context (data refs. [139, 140]).

11.3. AI-optimised microstructure design

AI-driven approaches using generative adversarial networks (GANs) and physics-informed neural networks (PINNs) for microstructure-property prediction and multi-objective optimisation are emerging as transformative development tools [112]. Cobalt-based MOF-derived CPCMs demonstrate that higher carbonisation temperatures improve graphitisation, broadband solar absorption, and thermal conductivity; molecular dynamics simulations reveal optimised structures reducing interfacial thermal resistance by 41.25% to 0.94×10^{-8} K m^2 W^{-1} [141]. Carboxyl-functionalised MWCNT/epoxy/n-docosane composites achieve 62% thermal conductivity improvement through stronger hydrogen bonding interactions confirmed by molecular dynamics [142]. Fig. 22 presents the AI-optimised microstructure design workflow.

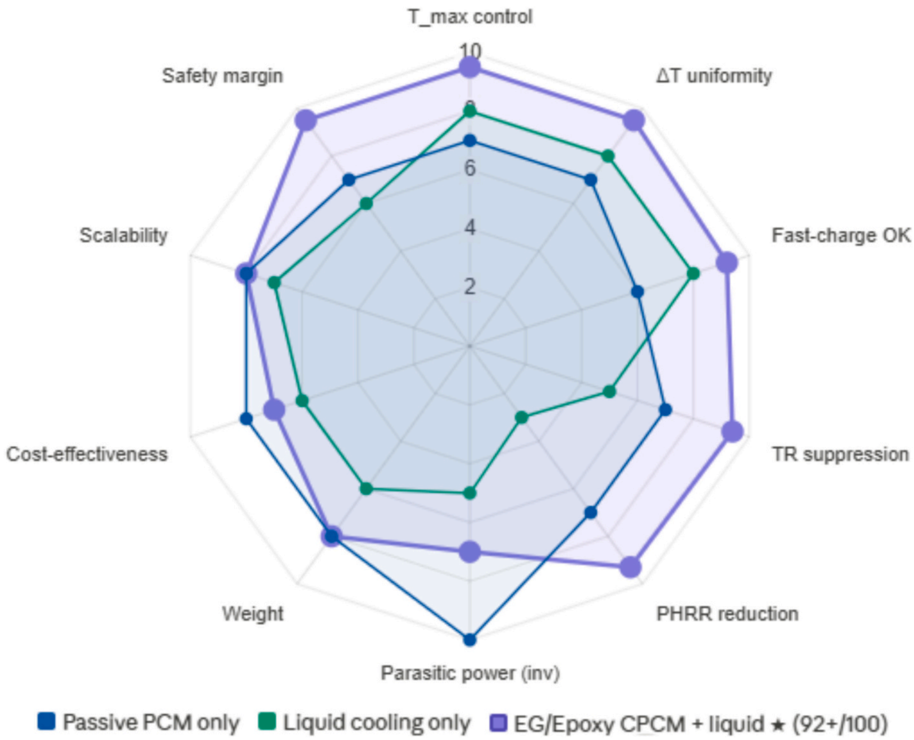

Fig. 18. Spider diagram illustrating hybrid BTMS performance comparison.

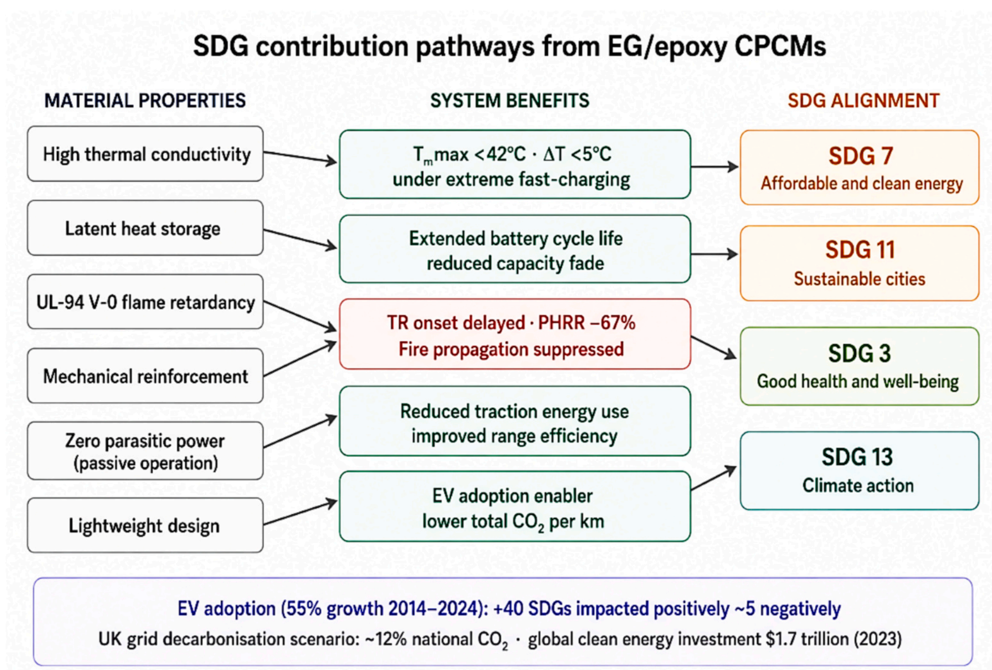

Fig. 19. Contribution of EG/epoxy CPCMs to SDG, showing pathways to reduced emissions, improved safety, and enhanced energy efficiency aligned with SDG 7 and SDG 11.

12. Conclusions

This review has critically examined EG and epoxy-reinforced CPCMs for EV battery thermal management through synthesis of 145+ peer-reviewed publications. The state-of-the-art developments in EG and epoxy resin-reinforced CPCMs for EV BTMS have been comprehensively assessed. The combination of the high-porosity conductive scaffold of EG and the structural and flame-retardant properties of the epoxy matrix overcomes the long-standing drawbacks of traditional PCMs (i.e., low thermal conductivity, leakage, and mechanical weakness). The following principal conclusions are drawn:

1. Thermal conductivity enhancement: EG-enhanced composites achieve $k = 27.10\ W\ m^{-1}\ K^{-1}$ exceeding pure paraffin by $>100\times$ with tensile and compressive strengths of 9.0 MPa and 39.4 MPa,

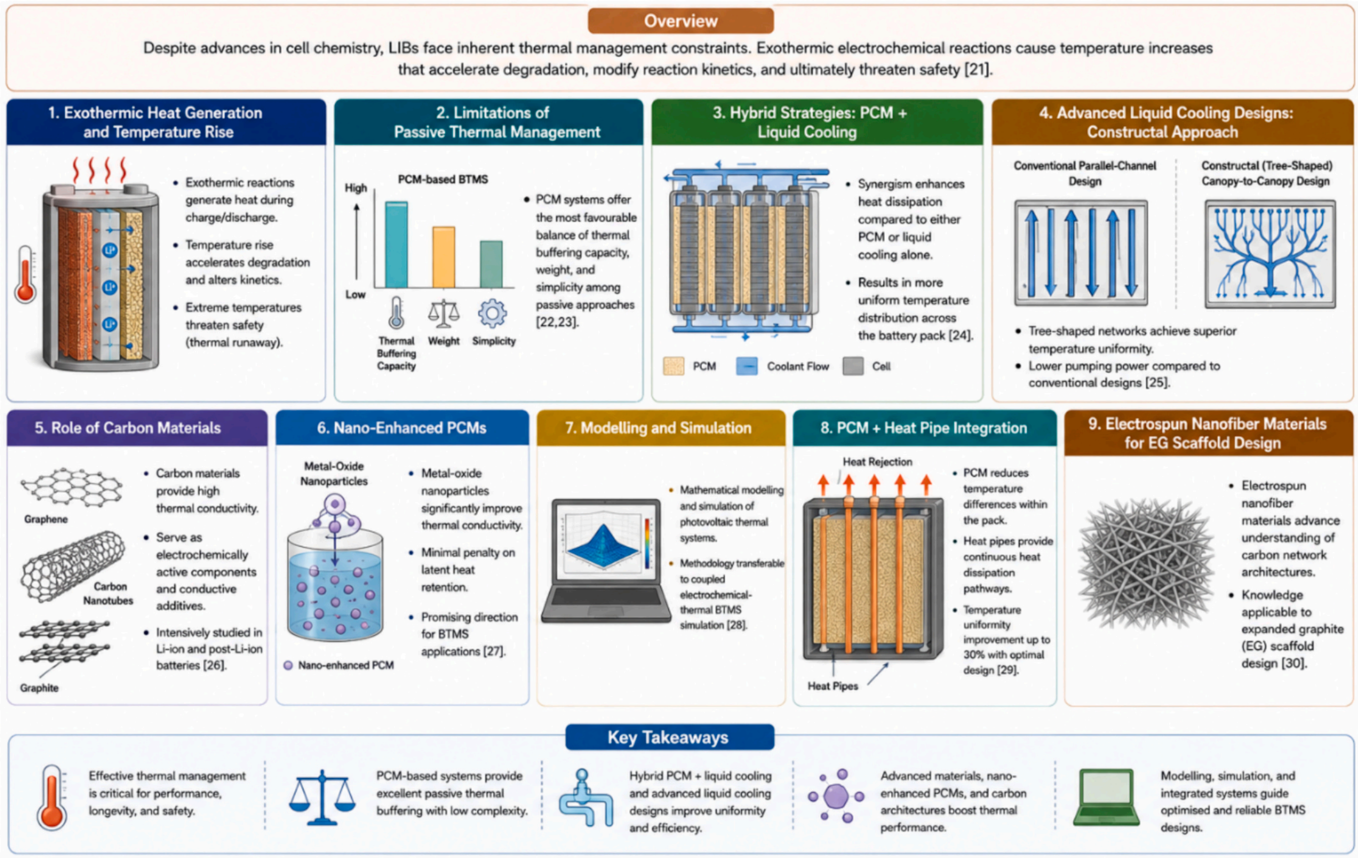

Fig. 20. Challenges, research gaps and future directions in BTMS in LIB.

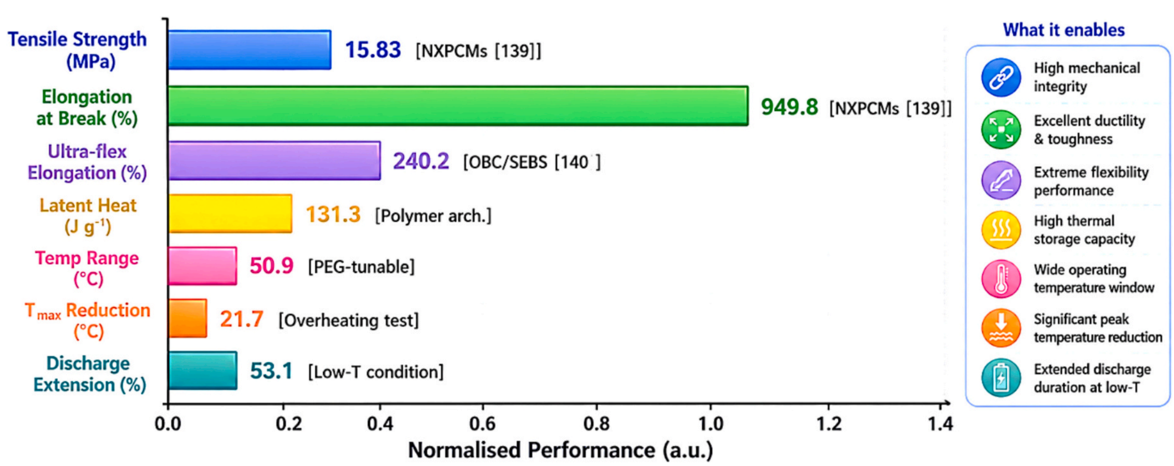

Fig. 21. Next-generation flexible CPCM properties in a solid-state battery context (data refs. [139, 140]).

maintaining battery surface temperatures below 42 °C under high-load operation.

2. Module-level performance: The 80/10/10 (PCM/EG/ER) SSPCM maintains 37.2 °C at 2 C and 50.5 °C at 4 C discharge, reducing peak temperature by 40% relative to air cooling. PSTE4 controls T_max and ΔT below 44.7 °C and 3.6 °C with anti-leakage with antileakage >99.9% at 70 °C.
3. Extreme fast-charging capability: Dual-phase PCM + EG (40 W m^{-1} K^{-1}) + ER + graphite film (1400 W m^{-1} K^{-1}) achieves T_max = 33 °C and ΔT = 1.4 °C at 4 C, with 44.8 °C after six extreme cycles.
4. Flame retardancy: ER/ATH/EG ternary composite achieves UL-94 V-0 classification with 67.33% PHRR reduction and 50.38% THR reduction alongside 400.12% increase in compression modulus.
5. Optimal formulation: CPCMs with 16–20 wt% EG offer the most promising shape-stabilised configuration; the 80/10/10 (PCM/EG/ER) mass ratio balances latent heat, conductivity, and mechanical integrity.
6. Sustainability: EV adoption positively impacts 40 SDGs; EG/epoxy CPCMs support SDG 7 and SDG 11 through lightweight, low-parasitic thermal management.
7. Future research: Flexible CPCMs for solid-state batteries, AI-optimised microstructure design using GANs/PINNs, and

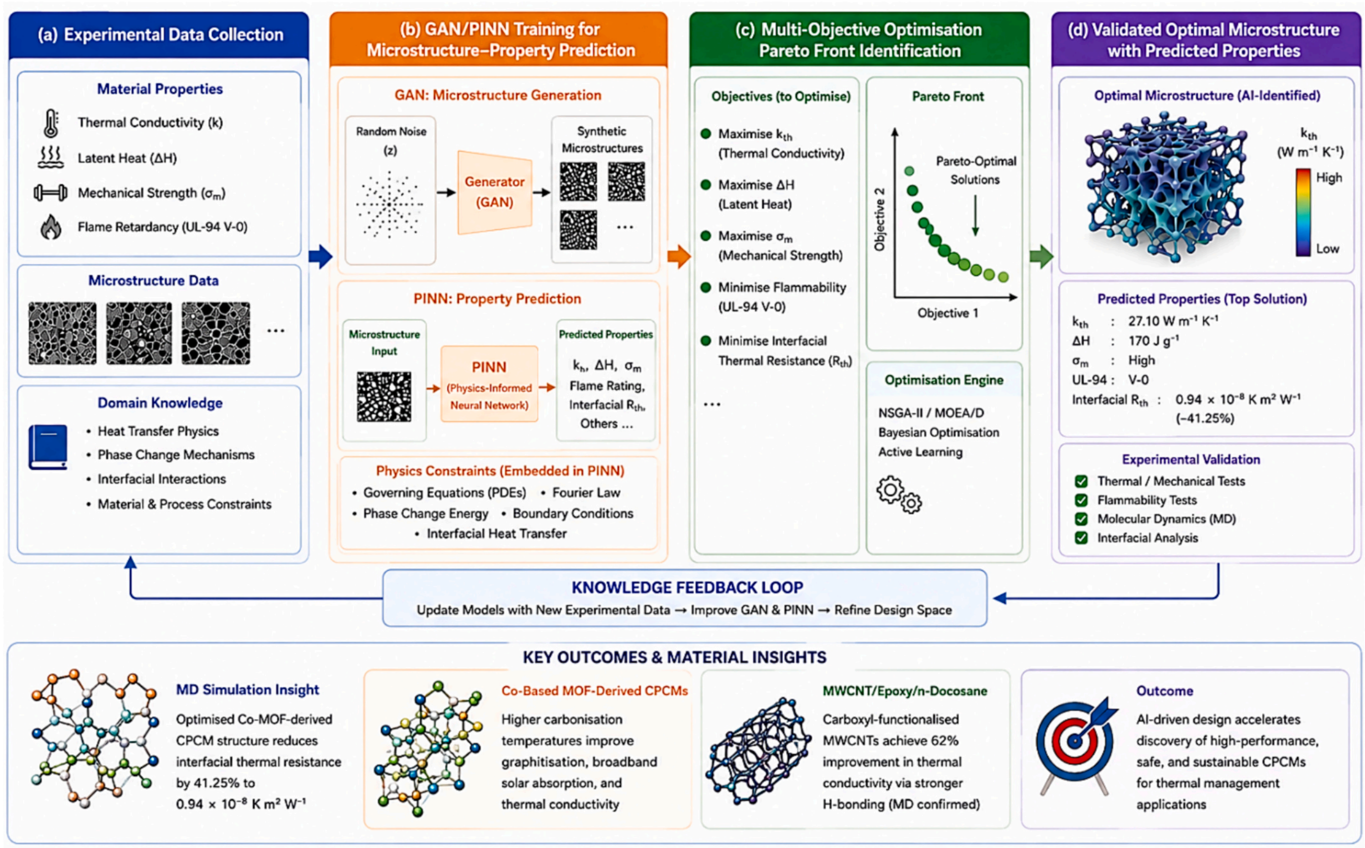

Fig. 22. AI-optimised microstructure design workflow for EG/epoxy CPCMs: (a) experimental data collection; (b) GAN/PINN training for microstructure-property prediction; (c) multi-objective optimisation Pareto front identification; (d) validated optimal microstructure with predicted properties.

interfacial thermal resistance reduction via functionalised nanofillers represent the most impactful near-term research frontiers.

EG/epoxy CPCMs constitute a transformative passive-dominant technology for next-generation EV BTMS, enabling safer, more efficient, and sustainable electrification at gigawatt-hour scale.

Abbreviations

ATH	aluminium trihydroxide
BTMS	battery thermal management system
CPCM	composite phase change material
DSC	differential scanning calorimetry
EG	expanded graphite
ER	epoxy resin
EV	electric vehicle
LFP	lithium iron phosphate
LIB	lithium-ion battery
LFA	laser flash analysis
NMC	nickel manganese cobalt oxide
OA	octadecanoic acid (stearic acid)
OL	octadecanol (stearyl alcohol)
OBC	olefin block copolymer
PA	palmitic acid (or polyamide per context)
PCM	phase change material
PHRR	peak heat release rate
SEI	solid electrolyte interphase
SSPCM	shape-stabilised phase change material
TGA	thermogravimetric analysis
THR	total heat release
TR	thermal runaway
UL-94	Underwriters Laboratories flammability standard 94

CRediT authorship contribution statement

R.M. Ghogare: Writing – original draft, Methodology, Investigation, Formal analysis, Conceptualization. **D.D. Deshmukh:** Supervision, Methodology, Investigation, Formal analysis, Review and editing of the manuscript.

Declaration of competing interest

The authors declare that they have no known competing financial interests or personal relationships that could have appeared to influence the work reported in this paper.

Data availability

Data will be made available on request.

References

[1] V.S.N. Reddy, B.N. Sai, A.S. Babu, A. Avinash, T.A. Rajesh, A.V.S. Manohar, A. Arif, Smart integration of expandable graphite in composite phase change materials for optimized electric vehicle battery thermal management, Heat Transf. 54 (7) (2025) 4745–4760.
[2] X. Zhang, J. Huo, X. Yuan, M. Zheng, S. Guo, Sulfur-free expanded graphite/paraffin composite phase change material with high thermal conductivity for lithium-ion battery thermal management, J. Therm. Sci. 34 (2025) 1287–1300.
[3] X. Luo, Q. Guo, X. Li, Z. Tao, S. Lei, J. Liu, L. Kang, D. Zheng, Z. Liu, Experimental investigation on a novel phase change material composite coupled with graphite film used for thermal management of lithium-ion batteries, Renew. Energy 145 (2019) 2046–2055.
[4] H.J.M. Pea, Z. An, X. Du, B. Fu, D. Zhang, X. Wang, Epoxy resin/aluminium hydroxide/expanded graphite synergistic effects on advancing flame retardancy,

mechanical structure and thermal management of octadecanoic acid and octadecanol-based eutectic phase change materials, Chem. Eng. J. 490 (2024) 151558.
[5] M. Muratori, D. Arent, M.D. Bazilian, J. Bistline, B. Borlaug, A. Brown, P. Cazzola, E.M. Dede, C. Gearhart, D. Greene, A. Jenn, Trends and 2025 insights on the rise of electric vehicles in the USA, Nat. Rev. Clean Technol. 1 (2025) 827–845.
[6] K.P. Srinivasa Perumal, L. Selvarajan, S.M. Sekar, E. Natarajan, Examining thermogravimetric response and morphological alterations in epoxy composites with hybrid ceramic fillers integration, Mater. Chem. Phys. 325 (2024) 129755.
[7] X. Zhao, X. Li, Y. Mao, J. Sun, Electric vehicle industry and sustainable economic growth: a measurement, coupling and causal analysis, Sustain. Fut. 8 (2024) 100242.
[8] X. Li, X. Zhao, D. Xue, Q. Tian, Impact of regional temperature on the adoption of electric vehicles: an empirical study based on 20 provinces in China, Environ. Sci. Pollut. Res. 30 (2022) 1–15.
[9] Z. Chen, K. Zhang, S. Jia, Influence factors and risk analysis of new energy vehicles from the perspective of system, Environ. Sci. Pollut. Res. 28 (2021) 1–16.
[10] B. Liu, C. Song, X. Liang, M. Lai, Z. Yu, J. Ji, Regional differences in China's electric vehicle sales forecasting: under supply-demand policy scenarios, Energy Policy 177 (2023) 113554.
[11] G. Huaying, H. Chaoqun, Analysis of China's pure electric vehicle sales based on spatial econometric models, Int. J. Econ. Financ. 13 (2020) 12.
[12] J. Shao, M. Misic, Why does electric vehicle deployment vary so much within a nation? Comparing Chinese provinces by policy, economics, and socio-demographics, Energy Res. Soc. Sci. 102 (2023) 103196.
[13] X. Shi, R. Jing, G.M. Hou, J.P. Wang, Network position advantage and technological innovation of China's new energy vehicle based on the perspective of network theory, Sustainability 11 (2019) 2098.
[14] B. Ashok, C. Kannan, B. Mason, S.D. Ashok, V. Indragandhi, D. Patel, A.S. Wagh, A.V. Jain, C. Kavitha, Towards safer and smarter design for lithium-ion-battery-powered electric vehicles: a comprehensive review on control strategy architecture of battery management system, Energies 15 (2022) 4227.
[15] Z. Wang, S. Yuan, S. Cai, R. Huang, Y. Liu, M. Wei, P. Zhang, J. Hu, Masked self-supervised transformer framework for state-of-health estimation of electric vehicle lithium batteries, Energy Fuel 40 (9) (2026) 4844–4863.
[16] K. Chidambaram, V. Rajasekar, K. Chinnadurai, B. Ashok, Critical review towards thermal management systems of lithium-ion batteries in electric vehicle with its electronic control unit and assessment tools, Proc. Inst. Mech. Eng. Pt. D J. Automob. Eng. 235 (2021) 095440702098286.
[17] P. Li, S. Luo, Y. Lin, J. Xiao, X. Xia, X. Liu, L. Wang, X. He, Fundamentals of the recycling of spent lithium-ion batteries, Chem. Soc. Rev. 53 (24) (2024) 11967–12013.
[18] W. Liu, T. Placke, K.T. Chau, Overview of batteries and battery management for electric vehicles, Energy Rep. 8 (2022) 4058–4084.
[19] T. Shams, M. Islam, W. Alam, M. Modak, S. Bin Hossain, V. Ramadesigan, M. Ahmed, H. Ahmed, A. Iqbal, A review of thermal management for Li-ion batteries: prospects, challenges, and issues, J. Energy Storage 39 (2021) 102518.
[20] K.Y. Gomez Diaz, S.E. De Leon Aldaco, J. Aguayo Alquicira, M. Ponce Silva, S. Portillo Contreras, O. Sanchez Vargas, Thermal management systems for lithium-ion batteries for electric vehicles: a review, World Electr. Veh. J. 16 (7) (2025) 346.
[21] S. Gungor, S. Gocmen, E. Cetkin, A review on battery thermal management strategies in lithium-ion and post-lithium batteries for electric vehicles, J. Ther. Eng. 9 (2023) 1078–1099.
[22] J. Luo, D. Zou, Y. Wang, S. Wang, L. Huang, Battery thermal management systems (BTMs) based on phase change material (PCM): a comprehensive review, Chem. Eng. J. 430 (2021) 132741.
[23] A. Wazeer, A. Das, C. Abeykoon, A. Sinha, A. Karmakar, Phase change materials for battery thermal management of electric and hybrid vehicles: a review, Energy Nexus 7 (2022) 100131.
[24] F. Yi, J. E, B. Zhang, H. Zuo, K. Wei, J. Chen, H. Zhu, H. Zhu, Y. Deng, Effects analysis on heat dissipation characteristics of lithium-ion battery thermal management system under the synergism of phase change material and liquid cooling method, Renew. Energy 181 (2022) 472–489.
[25] S. Gungor, E. Cetkin, S. Lorente, Canopy-to-canopy liquid cooling for the thermal management of lithium-ion batteries, a constructal approach, Int. J. Heat Mass Transf. 182 (2021) 121918.
[26] Y. Ahmad, M. Colin, C. Gervillie-Mouravieff, M. Dubois, K. Guerin, Carbon in lithium-ion and post-lithium-ion batteries: recent features, Synth. Met. 280 (2021) 116864.
[27] R. Jilte, A. Afzal, S. Panchal, A novel battery thermal management system using nano-enhanced phase change materials, Energy 219 (2020) 119564.
[28] T. Hajibeigy, R. Walvekar, C. Vaithilingam, Mathematical modelling, simulation analysis of a photovoltaic thermal system, J. Ther. Eng. 7 (2021) 291–306.
[29] K. Chen, J. Hou, M. Song, S. Wang, W. Wu, Y. Zhang, Design of battery thermal management system based on phase change material and heat pipe, Appl. Therm. Eng. 188 (2021) 116665.
[30] F. Shi, C. Chen, Z.L. Xu, Recent advances on electrospun nanofiber materials for post-lithium ion batteries, Adv. Fiber Mater. 3 (2021).
[31] Y. Li, X. Liu, L. Wang, X. Feng, D. Ren, Y. Wu, G. Xu, L. Lu, J. Hou, W. Zhang, Y. Wang, W. Xu, Y. Ren, Z. Wang, J. Huang, X. Meng, X. Han, H. Wang, X. He, M. Ouyang, Thermal runaway mechanism of lithium-ion battery with $LiNi_{0.8}Mn_{0.1}Co_{0.1}O_2$ cathode materials, Nano Energy 85 (2021) 105878.
[32] J. Hu, T. Liu, Q. Tang, X. Wang, Experimental investigation on thermal runaway propagation in the lithium ion battery modules under charging condition, Appl. Therm. Eng. 211 (2022) 118522.
[33] H. Shi, M. Cheng, Y. Feng, C. Qiu, C. Song, N. Yuan, C. Kang, K. Yang, J. Yuan, Y. Li, Thermal management techniques for lithium-ion batteries based on phase change materials: a systematic review and prospective recommendations, Energies 16 (2) (2023) 876.
[34] A. Calborean, L. Mathe, O. Bruj, Phase change materials for thermal management in lithium-ion battery packs: a review, Batteries 11 (12) (2025) 432.
[35] Q. Yue, C. He, H. Jiang, M. Wu, T. Zhao, A hybrid battery thermal management system for electric vehicles under dynamic working conditions, Int. J. Heat Mass Transf. 164 (2020) 120528.
[36] H. Yang, G. Zhang, B. Dou, X. Yan, W. Lu, Z. Wu, Q. Yang, Review on the lithium-ion battery thermal management system based on composite phase change materials: progress and outlook, Energy Fuel 38 (4) (2024) 2573–2600.
[37] M. Wu, X. Li, X. Mei, Y. Zhang, J. Zhang, C. Zheng, J.P. Xue, L. Zhou, In situ polymerization of 1,3-dioxane in solid-state lithium batteries: a mini-review of recent developments, Energy Fuel 39 (27) (2025) 12830–12846.
[38] M.G. Kibria, M.S. Mohtasim, U.K. Paul, I.A. Fahim, Nafi, B.K. Das, H. A. Mohammed, A review on composite phase change materials and fins-based Li-ion battery thermal management systems with design perspectives and future outlooks, Energy Fuel 38 (15) (2024) 13637–13660.
[39] S.S. Kumar, G.A.P. Rao, Recent progress on battery thermal management with composite phase change materials, Energy Storage 6 (4) (2024).
[40] K. Li, J. Guo, T. Wu, et al., Development of phase change material for thermal management of lithium-ion batteries: a review, J. Therm. Anal. Calorim. 150 (2025) 17947–17972.
[41] M.G. Rani, R. Rangasamy, Review of phase change material application in thermal management of electric vehicle battery pack, Proc. Inst. Mech. Eng. A J. Power Energy 238 (1) (2023) 197–214.
[42] G. Rasool, W. Xinhua, T. Sun, T. Hayat, M. Sheremet, A. Uddin, H. Shahzad, K. Abbas, I. Razzaq, W. Yuexin, Recent advancements in battery thermal management system (BTMS): a review of performance enhancement techniques with an emphasis on nano-enhanced phase change materials, Heliyon 10 (17) (2024) e36950.
[43] M. Nasiri, H. Hadim, Thermal management of Li-ion batteries using phase change materials: recent advances and future challenges, J. Energy Storage 111 (2025) 115440.
[44] X. Guo, Y. Zhang, J. Li, et al., Wet spinning technology for aerogel fiber: pioneering the frontier of high-performance and multifunctional materials, Adv. Fiber Mater. 6 (2024) 1669–1709.
[45] I.U. Rahman, S. Nardini, B. Buonomo, H.J. Mohammed, H. Khan, S.U. Rehman, O. Manca, Graphene-enhanced composite phase change materials for battery thermal management, in: Nanotechnology and Nanomaterials, 2025.
[46] M. Abushuhel, M.H. Abdellattif, S.K. Saraswat, A.F. Al-Hussainy, S. Mohammed, M. Nourizadeh, Electrochemical-thermal modeling of NMC811 lithium-ion batteries to analyze temperature rise characteristics at different discharge rates, Int. J. Electrochem. Sci. 20 (11) (2025) 101176.
[47] S. Liu, J. Zhao, S. Lu, Q. Zhou, C. Ruan, H. Zhang, In-situ measurement of heat generation and thermal behavior of cyclic aged $LiFePO_4$ batteries, J. Energy Storage 143 (2025) 119693.
[48] L. Sheng, C. Zhang, J. Xu, Q. Zhou, X. Zhang, Quantitative measurement of thermal performance of a cylindrical lithium-ion battery, Measurement 239 (2024) 115458.
[49] X. Lin, K. Khosravinia, X. Hu, J. Li, W. Lu, Lithium plating mechanism, detection, and mitigation in lithium-ion batteries, Prog. Energy Combust. Sci. 87 (2021) 100953.
[50] A.S. Mussa, A.J. Smith, G.M. Trippetta, G. Lindbergh, M. Klett, R.W. Lindstrom, Performance and aging of a lithium-ion battery in a non-uniform temperature distribution condition, J. Energy Storage 114 (2025) 115869.
[51] Y. Troxler, B. Wu, M. Marinescu, V. Yufit, Y. Patel, A. Marquis, N. Brandon, G. Offer, The effect of thermal gradients on the performance of lithium-ion batteries, J. Power Sources 247 (2013) 1018–1025.
[52] J.C. Hestenes, J.T. Sadowski, R. May, L.E. Marbella, Transition metal dissolution mechanisms and impacts on electronic conductivity in composite $LiNi_{0.5}Mn_{1.5}O_4$ cathode films, ACS Mater. Au 3 (2) (2022) 88–101.
[53] F. Novotny, S. Baumbach, W. Tegethoff, A. Golubkov, J. Rieser, J. Kohler, Evaluation of the released energy during a thermal runaway of prismatic lithium-ion batteries using a novel cyclone-calorimetry approach, J. Electrochem. Soc. 172 (12) (2025) 120501.
[54] L. Sun, C. Wei, D. Guo, J. Liu, Z. Zhao, Z. Zheng, Y. Jin, Comparative study on thermal runaway characteristics of lithium iron phosphate battery modules under different overcharge conditions, Fire Technol. 56 (2020).
[55] P. Lyu, G. Chen, X. Liu, M. Li, Z. Rao, Mitigating thermal runaway propagation for lithium-ion batteries by a novel integrated liquid cooling/aerogel strategies, Appl. Therm. Eng. 269 (2025) 126001.
[56] P. Yadav, L. Jinadasa, A. Wray, S. Petrovich, M. Georgiou, K. Ebrahimi, Battery electric vehicle thermal management system modelling and validation, Thermo 6 (1) (2026) 4.
[57] C. Reiter, N. Wassiliadis, M. Lienkamp, Design of thermal management systems for battery electric vehicles, in: 2019 Fourteenth International Conference on Ecological Vehicles and Renewable Energies (EVER), IEEE, 2019, pp. 1–10.
[58] X. Liu, Y. Xia, Y. Hong, Z. Zhu, K. Shen, J. Wang, X. Li, F. Dai, J. Hua, Y. Sun, Y. Zheng, Thermal barrier for preventing battery thermal runaway propagation: sensitivity analysis of parameters and suppression strategy, J. Energy Storage 141 (2025) 119501.
[59] L. Zhou, S. Zhang, A. Jain, X. Li, Recent advances in indirect liquid cooling of lithium-ion batteries, J. Energy Storage 132 (2025) 117750.

[60] S.P. Verma, S. Saraswati, Comprehensive thermal performance analysis of an air-cooled staggered configured Li-ion battery pack: a numerical and experimental approach, J. Energy Storage 89 (2024) 111792.
[61] C. Li, Y. Wang, Z. Sun, X. Wen, J. Wu, L. Feng, D. Liu, Two-phase immersion liquid cooling system for 4680 Li-ion battery thermal management, J. Energy Storage 97 (2024) 112952.
[62] D. Luo, L. Jiang, H. Chen, et al., Thermoelectric-based battery thermal management with cooling and energy recovery, Innov. Energy 3 (2026) 100134.
[63] S.M.D. Shehabaz, S.K. Gugulothu, R. Muthyala, P. Barmavatu, Enhanced thermal regulation of lithium-ion batteries using composite phase change material-FIN structures for high heat dissipation, J. Ther. Sci. Eng. Appl. 17 (4) (2025).
[64] R.G. Chi, S.H. Rhi, Oscillating heat pipe cooling system of electric vehicle's Li-ion batteries with direct contact bottom cooling mode, Energies 12 (9) (2019) 1698.
[65] P.S. Shinde, P. Naik, Heat-pipe-assisted air cooling of lithium-titanate prismatic battery, J. Ther. Sci. Eng. Appl. 15 (2) (2022).
[66] M. Hao, J. Li, S. Park, et al., Efficient thermal management of Li-ion batteries with a passive interfacial thermal regulator based on a shape memory alloy, Nat. Energy 3 (2018) 899–906.
[67] L. Spitthoff, P.R. Shearing, O.S. Burheim, Temperature, ageing and thermal management of lithium-ion batteries, Energies 14 (5) (2021) 1248.
[68] K. Boonma, N. Patimaporntap, H. Mbulu, P. Trinuruk, K. Ruangjirakit, Y. Laoonual, S. Wongwises, A review of the parameters affecting a heat pipe thermal management system for lithium-ion batteries, Energies 15 (22) (2022) 8534.
[69] D. Karimi, H. Behi, J. Van Mierlo, M. Berecibar, Novel hybrid thermal management system for high-power lithium-ion module for electric vehicles: fast charging applications, World Electr. Veh. J. 13 (5) (2022) 86.
[70] S. Vikram, S. Vashisht, D. Rakshit, M.P. Wan, Recent advancements and performance implications of hybrid battery thermal management systems for electric vehicles, J. Energy Storage 90 (2024) 111814.
[71] H. Zhou, W. Li, D. Gong, C. Xue, X. Guo, Z. Song, Thermal performance of a hybrid thermal management system that couples PCM with liquid cooling for cylindrical lithium-ion battery, Appl. Therm. Eng. 274 (2025) 126736.
[72] M. Amer, M. Sameh, A. Hamed, M. Shouman, Experimental comparative study of passive, active, and hybrid battery thermal management systems for fast discharge in hot environments, Appl. Therm. Eng. 291 (2026) 130209.
[73] M. Al Qubeissi, A. Mahmoud, M. Al-Damook, A. Almshahy, Z. Khatir, H. S. Soyhan, R.M. Raja Ahsan Shah, Comparative analysis of battery thermal management system using biodiesel fuels, Energies 16 (1) (2023) 565.
[74] D. Paul, A. Nandi, S. Bhattacharyya, et al., A comprehensive review on lithium-ion battery thermal management (BTM) using phase change materials: advances, challenges, and future perspectives, J. Therm. Anal. Calorim. 150 (2025) 9669–9722.
[75] A. Boretti, Advanced battery thermal management: a review of materials, cooling systems, and intelligent control for safety and performance, Energy Storage 7 (7) (2025).
[76] Z. Wu, Z. Wang, M. Wang, et al., Preparation of sandwich-structured thermally conductive and insulating composite materials based on electrospinning combined with hot pressing technology, Adv. Compos. Hybrid Mater. 8 (2025) 69.
[77] S. Jiong, J. Kim, K. Kim, et al., Electrostatically engineered thermal interface materials with multiscale boron nitride-alumina-nanodiamond fillers in polyvinyl alcohol composites for tailored anisotropic thermal conductivities, Adv. Compos. Hybrid Mater. 8 (2025) 321.
[78] M. Malik, I. Dincer, M.A. Rosen, Review on use of phase change materials in battery thermal management for electric and hybrid electric vehicles, Int. J. Energy Res. 40 (8) (2016) 1011–1031.
[79] R. Bidiyasar, R. Kumar, N. Jakhar, A critical review of polymer support-based shape-stabilized phase change materials for thermal energy storage applications, Energy Storage 6 (4) (2024).
[80] N. Napa, M.K. Agrawal, B. Tamma, Impact of active and passive thermal management strategies on the ageing of lithium-ion battery module under constant and monthly average ambient temperature, J. Energy Storage 113 (2025) 115642.
[81] M.H. Zahir, S.A. Mohamed, R. Saidur, F.A. Al-Sulaiman, Supercooling of phase-change materials and the techniques used to mitigate the phenomenon, Appl. Energy 240 (2019) 793–817.
[82] J. Xu, Highly thermally conductive and flexible phase change composites enabled by polymer/graphite nanoplatelet-based dual networks for efficient thermal management, J. Mater. Chem. A 8 (2020).
[83] H.J. Mombeki Pea, Z. An, X. Du, et al., Structure, characterization and thermal properties of the form-stable paraffin/high-density polyethylene/expanded graphite/epoxy resin composite PCMs for thermal energy storage, J. Therm. Sci. 32 (2023) 2104–2114.
[84] Y. Zhao, S. Huang, Z. Jin, Z. Xie, H. Guo, H. Xie, Thermally conductive shape-stabilized phase change materials enabled by paraffin wax and nanoporous structural expanded graphite, Nanomaterials 15 (2) (2025) 110.
[85] X. Wang, B. Li, Z. Qu, J. Zhang, Z. Jin, Effects of graphite microstructure evolution on the anisotropic thermal conductivity of expanded graphite/paraffin phase change materials and their thermal energy storage performance, Int. J. Heat Mass Transf. 155 (2020) 119853.
[86] G. Zhang, Y. Sun, C. Wu, X. Yan, W. Zhao, C. Peng, Low-cost and highly thermally conductive lauric acid-paraffin-expanded graphite multifunctional composite phase change materials for quenching thermal runaway of lithium-ion battery, Energy Rep. 9 (2023) 2538–2547.
[87] X. Lin, X. Zhang, L. Liu, J. Liang, W. Liu, Polymer/expanded graphite-based flexible phase change material with high thermal conductivity for battery thermal management, J. Clean. Prod. 331 (2021) 130014.
[88] C. Li, X. Wu, S. Li, W. Yang, S. Wu, X. Liu, X. Li, Research on the high thermal conductivity composite phase change materials with graphite nanosheets for battery thermal safety, J. Energy Storage 61 (2023) 106718.
[89] S.W. Hyun, Y.J. Kim, J.H. Lee, Enhanced safety of high-power lithium-ion batteries using thermally conductive and flame-retardant shape-stabilized PCM composed of organic PCM, epoxy resin, and expanded graphite, Appl. Therm. Eng. 265 (2025) 125064.
[90] K. Yang, Z. Ling, X. Fang, Z. Zhang, Introducing a flexible insulation network to the expanded graphite-based composite phase change material to enhance dielectric and mechanical properties for battery thermal management, J. Energy Storage 66 (2023) 107486.
[91] Z. Leng, X. Cao, W. Zhong, C. Zeng, Heat pipe/phase change material coupled thermal management in Li-ion battery packs: optimization and energy-saving assessment, Appl. Therm. Eng. 208 (2022) 118211.
[92] D. Zhou, J. Yuan, Y. Zhou, et al., Preparation and characterization of myristic acid/expanded graphite composite phase change materials for thermal energy storage, Sci. Rep. 10 (2020) 10889.
[93] Y. Cui, Y. Chen, L. Zhao, F. Zhu, L. Li, Q. Kong, M. Chen, Investigation on the properties of flame-retardant phase change material and its application in battery thermal management, Energies 16 (1) (2023) 521.
[94] S.K. Chung, Y. Jo, S. Baik, S. Kang, K. Choi, Enhanced battery thermal management by conventional heatsinks integrated with thermoelectric module and multi-layered phase change materials, SSRN Electron. J. (2025). Available at SSRN 5261327.
[95] W. Yang, X. Li, C. Li, J. Deng, Y. Du, G. Zhang, High antileakage and thermal conductivity composite phase-change material with anisotropy expanded graphite for battery thermal management, ACS Appl. Energy Mater. 6 (18) (2023) 9698–9708.
[96] G. Jiang, J. Huang, Y. Fu, M. Cao, M. Liu, Thermal optimization of composite phase change material/expanded graphite for Li-ion battery thermal management, Appl. Therm. Eng. 108 (2016) 1119–1125.
[97] G.K. Marri, Y.J. Ee, Z. He, J.Y. Ho, High-performance moldable composite phase change material for scalable external thermoregulation of Li-ion batteries, Appl. Therm. Eng. 279 (2025) 127954.
[98] D. K, V. Varma, P. Govindarajan, R. Ramanujan, Hybrid thermomagnetic oscillator for cooling and direct waste heat conversion to electricity, Appl. Energy 233–234 (2018) 312–320.
[99] L. Qian, W. Xiao, G. Fei, C. Xia, Y. Yi, T. Ma, S. Chen, Immersion cooling control for ununiform degraded lithium-ion batteries under fast charging, J. Energy Storage 153 (2026) 120820.
[100] F. Ma, Y. Liang, Z. Tao, X. Guo, Q. Guo, Z. Liu, A novel PCM/expanded graphite composite sphere with high thermal conductivity and excellent shape stability used for a packed-bed thermal energy system, Diam. Relat. Mater. 145 (2024) 111102.
[101] G. Cheng, Z. Wang, X. Wang, Y. He, All-climate thermal management structure for batteries based on expanded graphite/polymer composite phase change material with a high thermal and electrical conductivity, Appl. Energy 322 (2022) 119509.
[102] W. Yang, R. Lin, X. Li, C. Li, Y. Wu, G. Zhang, et al., High thermal conductive and anti-leakage composite phase change material with halloysite nanotube for battery thermal management system, J. Energy Storage 66 (2023) 107372.
[103] J. Li, W. Duan, Y. Chen, H. Chen, M. Song, S. Liao, et al., Thermal performance of pin fin heat sinks with phase change material for electronic devices thermal management, Appl. Therm. Eng. 250 (2024) 123456.
[104] H.J. Mombeki Pea, Z. An, X. Du, W. Hou, D. Zhang, X. Liu, Experimental and analytical studies on latent heat of hydrated salt/modified EG-based form-stable composite PCMs for energy storage application, Renew. Energy 222 (2024) 119978.
[105] H. Liang, H. Wang, P. Zhang, D. Ding, Y. Jiao, Y. Zhou, Q. Xue, Q. Song, Q. Zhang, Y. Chen, Phase change materials encapsulated in a novel hybrid carbon skeleton for high-efficiency solar-thermal conversion and energy storage, J. Energy Storage 86 (2024) 111307.
[106] H. Yang, M. Li, Z. Wang, B. Ma, A compact and lightweight hybrid liquid cooling system coupling with Z-type cold plates and PCM composite for battery thermal management, Energy 263 (2022) 126026.
[107] L. Mingyun, J. Cao, N. Liu, Z. Zhang, Experimental and simulative investigations on a water immersion cooling system for cylindrical battery cells, Front. Energy Res. 10 (2022).
[108] S. Basu, K.S. Hariharan, S.M. Kolake, T. Song, D.K. Sohn, T. Yeo, Coupled electrochemical thermal modelling of a novel Li-ion battery pack thermal management system, Appl. Energy 181 (2016) 1–13.
[109] Z. An, H. Zhong, H. Liu, Z. Gao, Performance evaluation on liquid-PCM hybrid battery thermal management with spatial network flow channels, J. Energy Storage 118 (2025) 116251.
[110] J. Wang, B. Liu, X. Ding, Q. Li, B. Yu, U. Desideri, Multi-objective topology optimization design of nanofluid cooling plate for thermal management of lithium ion battery pack, Energy 337 (2025) 138600.
[111] W. Li, T. Yang, L. Chen, J. Shi, T. Zhang, C. Zeng, R. Liu, S. Tang, Thermal management study of cylindrical battery using novel thermally conductive anisotropic flexible phase change material, Case Stud. Therm. Eng. 73 (2025) 106508.
[112] Y. Nandakishora, N. Khayum, C. Patra, et al., AI driven approaches in battery thermal management systems for prediction and multi objective optimization: a comprehensive literature review, Discov. Mech. Eng. 5 (2026) 53.

[113] A.A. Arefin, S.T. Meraj, M.H. Lipu, M.S. Rahman, T. Rahman, K. Hasan, K. M. Muttaqi, Societal, environmental, and economic impacts of electric vehicles towards achieving sustainable development goals, Results Eng. 27 (2025) 1–19, 107060.
[114] G. Milev, A. Al-Habaibeh, D. Shin, Impact of replacing conventional cars with electric vehicles on UK electricity grid and carbon emissions, in: Springer Proceedings in Energy, 2021, pp. 199–206.
[115] A. Usman, S. Ullah, I. Ozturk, S. Sohail, M.T. Sohail, Does environmental policy stringency reduce trade in energy resources? Insights from coal, petroleum, and gas, Res. Policy 89 (2024) 104679.
[116] B. Shakmak, M. Watkins, A. Al-Habaibeh, How clean is the air you breathe? Air quality during commuting using various transport modes in Nottingham, in: Energy and Sustainable Futures: Proceedings of 2nd ICESF, Springer International Publishing, Cham, 2020, pp. 247–254.
[117] R. Marquez, C. Ovalles, F. Lopez-Linares, W. Wang, P. Robinson, M.A. Reynolds, Perspective from the ACS Energy & Fuels Industry Committee toward the transition to sustainable energy sources, Energy Fuel 39 (3) (2025) 1451–1459.
[118] B. Gudlaugsson, H. Dawood, G. Pillai, M. Short, First step towards a system dynamic sustainability assessment model for urban energy transition, in: Energy and Sustainable Futures: Proceedings of 2nd ICESF, Springer International Publishing, Cham, 2020, pp. 225–232.
[119] G. Last, D.E. Agbro, A. Asthana, The future of hybrid electric vehicles and sustainable vehicles in the UK, in: Energy and Sustainable Futures: Proceedings of 2nd ICESF, Springer International Publishing, Cham, 2020, pp. 213–221.
[120] M. Peacock, A. Fragaki, B.J. Matuszewski, Review of heat demand time series generation for energy system modelling, in: Springer Proceedings in Energy, 2021.
[121] J. Zhao, Y. Chen, M. Chen, Battery thermal management with a modified metal alloy/expanded graphite/paraffin composite phase change material, J. Energy Storage 113 (2025) 115652.
[122] A. Al-Mahmodi, Y. Manusamy, M. Atta, I. Suyambulingam, A. Bin Mokaizh, M. Muniyadi, Utilizing phase change materials in thermal energy systems: applications in waste heat recovery, Appl. Therm. Eng. 279 (2025) 128003.
[123] Gegentana, L. Cui, L. Zhou, X. Du, Deep potential molecular dynamics systematic study of microstructure and thermophysical properties of NaCl-$CaCl_2$ molten salt system across phase transition temperature, J. Therm. Sci. 33 (2024).
[124] G. Wie-Addo, A. Jones, S. Palmer, V. Starinieri, J. Renshaw, P. Bingham, Reformulating ceramic body composition to improve energy efficiency in brick manufacture, in: Energy and Sustainable Futures, 2021.
[125] S. Kartik, et al., Distributed activation energy model for thermal decomposition of polypropylene waste, in: Energy and Sustainable Futures, Springer, Cham, 2021.
[126] V. Dudhee, V. Vukovic, Integration of building information modelling and augmented reality for building energy systems visualisation, in: Energy and Sustainable Futures, 2021.
[127] S. Ferahtia, A. Houari, T. Cioara, M. Bouznit, H. Rezk, A. Djerioui, Recent advances on energy management and control of direct current microgrid for smart cities and industry: a survey, Appl. Energy 368 (2024) 123501.
[128] K.R. Khalilpour, A. Vassallo, A generic framework for distributed multi-generation and multi-storage energy systems, Energy 114 (2016) 798–813.
[129] F. Bai, M. Chen, W. Song, Z. Feng, Y. Li, Y. Ding, Thermal management performances of PCM/water cooling-plate using for lithium-ion battery module based on non-uniform internal heat source, Appl. Therm. Eng. 126 (2017) 17–27.
[130] G. Naresh, T.P. Kumar, B. Aadhithyan, S. Utkarsh, J.V. Nithin, Transient thermal analysis of passive air-cooled battery-pack for various casing material, IOP Conf. Ser.: Mater. Sci. Eng. 993 (1) (2020) 012131.
[131] F. Pra, J. Al Koussa, S. Ludwig, C.M. De Servi, Experimental and numerical investigation of the thermal performance of a hybrid battery thermal management system for an electric van, Batteries 7 (2) (2021) 27.
[132] H. Ekstrom, B. Fridholm, G. Lindbergh, Comparison of lumped diffusion models for voltage prediction of a lithium-ion battery cell during dynamic loads, J. Power Sources 402 (2018) 296–300.
[133] J. Deng, Q. Huang, X. Li, G. Zhang, C. Li, S. Li, Influence mechanism of battery thermal management with flexible flame-retardant composite phase change materials by temperature aging, Renew. Energy 222 (2023) 119922.
[134] C. Zhang, J. Huang, W. Sun, X. Xu, Y. Li, Research on the influence of liquid on heat dissipation and heating characteristics of lithium-ion battery thermal management system, World Electr. Veh. J. 13 (4) (2022) 68.
[135] M. Thabet, D. Sanders, N. Bausch, Detection of patterns in pressure signal of compressed air system using wavelet transform, in: Springer Proceedings in Energy, 2021, pp. 61–67.
[136] Z. Gao, F. Deng, D. Yan, H. Zhu, Z. An, P. Sun, Thermal performance of thermal management system coupling composite phase change material to water cooling with double s-shaped micro-channels for prismatic lithium-ion battery, J. Energy Storage 45 (2021) 103490.
[137] M. Malik, I. Dincer, M.A. Rosen, M. Mathew, M. Fowler, Thermal and electrical performance evaluations of series connected Li-ion batteries in a pack with liquid cooling, Appl. Therm. Eng. 129 (2017) 472–481.
[138] Y. Xia, H. Hao, G. Zanardo, A. Deeks, Long term vibration monitoring of an RC slab: temperature and humidity effect, Eng. Struct. 28 (3) (2005) 441–452.
[139] G. Zhu, J. Wang, W. Luo, W. Chen, Y. Ma, X. Jiang, et al., Solid-solid phase change films with intrinsic flexibility and photo-thermal conversion capabilities for human thermal management, Sol. Energy Mater. Sol. Cells 298 (2026) 114158.
[140] J. Wang, W. Luo, M. Zou, W. Chen, G. Zhu, S. Tan, et al., Ultra-flexible, adaptable and multifunctional polymer-based composite phase change materials for full-stage battery thermal management, Compos. Pt. B Eng. 313 (2026) 113416.
[141] Y. Liu, M. Zou, Y. Ma, W. Chen, Q. Li, X. Jiang, X. Hu, Effect of carbonization temperature on the photo-magnetic-thermal properties of cobalt-based metal organic framework-derived composite phase change materials: experimental and molecular dynamics simulations, Mater. Today Phys. 60 (2026) 101996.
[142] B. Fu, M. Zou, W. Luo, G. Zhu, J. Wang, C. Qiang, et al., Experimental research and molecular dynamics simulation of composite phase change materials based on functionalized carbon nanotubes/epoxy resin/n-docosane, Sol. Energy Mater. Sol. Cells 296 (2026) 114088.